CYTOKINE SIGNALING

Structural basis of γ chain family receptor sharing at the membrane level

Tiantian Cai[1]†‡, Rachel Lenoir Capello[1]†, Xiong Pi[1,2], Hao Wu[1,2], James J. Chou[1]*§

Common γ chain (γc) cytokine receptors, including interleukin-2 (IL-2), IL-4, IL-7, IL-9, IL-15, and IL-21 receptors, are activated upon engagement with a common γc receptor (CD132) by concomitant binding of their ectodomains to an interleukin. In this work, we find that direct interactions between the transmembrane domains (TMDs) of both the γc and the interleukin receptors (ILRs) are also required for receptor activation. Moreover, the same γc TMD can specifically recognize multiple ILR TMDs of diverse sequences within the family. Heterodimer structures of γc TMD bound to IL-7 and IL-9 receptor TMDs—determined in a lipid bilayer–like environment by nuclear magnetic resonance spectroscopy—reveal a conserved knob-into-hole mechanism of recognition that mediates receptor sharing within the membrane. Thus, signaling in the γc receptor family requires specific heterotypic interactions of the TMDs.

Members of the common γ chain (γc) family of cytokine receptors, upon binding to their corresponding interleukin, pair specifically with a common, shared γc receptor (CD132) to allow signal transduction (*1*, *2*). To date, the family consists of six members: the interleukin-2 receptor (IL-2R), IL-4R, IL-7R, IL-9R, IL-15R, and IL-21R. These receptors play crucial roles in the development and proliferation of multiple lymphocyte lineages of both the innate and adaptive immune systems (*1*, *3*) and are clinically important targets for immunotherapy (*2*, *4*, *5*). Interleukin receptors (ILRs) and the γc are type I transmembrane proteins comprising a ligand-binding ectodomain, a transmembrane domain (TMD), and an intracellular domain (ICD) containing a Janus kinase (JAK)–binding site.

The mechanism by which interleukins mediate specific pairing of the γc with ILRs has been revealed by crystallographic studies of the IL-2–bound and IL-4–bound receptor complexes (*6*–*8*). In both cases, the interleukin binding to an ILR generates a composite surface for subsequent interaction with the γc. This interaction interface is small (~1000 Å^2) and characterized by relatively flat surface complementarity (*7*), constituting the structural basis for the degenerate cytokine recognition by the γc.

One aspect of ILRs not well understood is the TMD and its possible role in receptor signaling. This question was inspired by previous studies on other receptors that have revealed much more active roles of TMDs in mediating receptor oligomerization and activation than conventionally appreciated. Examples include type 1 cytokine receptors, such as erythropoietin receptor (*9*), thrombopoietin receptor (*10*), growth hormone receptor (*11*, *12*), receptors in the tumor necrosis factor receptor superfamily (*13*, *14*), and receptor tyrosine kinases (*15*, *16*). An early cryo–electron microscopy (cryo-EM) study of a full-length transmembrane form of a quaternary cytokine-receptor complex comprising gp130, LIF-R, the cytokine ciliary neurotrophic factor (CNTF), and its alpha receptor (CNTF-Rα) has suggested that the TMDs of these receptor chains are associated (*17*). Furthermore, mutations within TMDs of the γc family receptors have been recorded in clinical studies. For example, a single mutation (V253G) in the IL-7R TMD is associated with acute lymphoblastic leukemias (ALLs) (*18*). The structural basis of these disease mutations is unknown owing to a lack of structural information for the transmembrane region of the γc family receptors.

In this study, we report that heterotypic interactions between the TMDs of the γc and its family members are an essential component of receptor signaling, which raises the question how a single transmembrane helix (TMH) can have the structural sophistication to specifically recognize a variety of TMHs with highly divergent sequences. We determined high-resolution structures of the γc TMD in complex with IL-7R and IL-9R TMDs in bicelles that mimic a lipid bilayer. The two heterodimer structures and functional mutagenesis reveal a common knob-into-hole mechanism that underlies degenerate ILR pairing with the γc within the membrane.

Removal of an ILR (IL-7R or IL-9R) and γc ectodomains activates JAK-STAT signaling

A large body of structural and functional studies on members of the γc family receptors have described receptor activation (*4*, *6*–*8*, *19*). Briefly, interleukins bind to the ectodomains of their α or β chain receptors to form a c[illegible] plex that subsequently recruits the γc, [illegible] positioning the ICDs in the correct arrangement to allow reciprocal phosphorylation of JAK1 and JAK3 and to activate downstream signal transducers and activators of transcription (STAT) signaling (Fig. 1A). However, the ectodomain and ICD are separated by the TMD, which may also contribute to driving a signaling-compatible configuration. The pre-ligand conformation of receptor ectodomains could physically prevent ligand-independent, TMD-driven signaling (*14*, *20*). To test whether heterotypic association between the ILR TMD and the γc TMD can be achieved by the removal of ectodomains, wild-type (WT) or cleavable human IL-7R (hIL-7R) and γc were designed (Fig. 1B) and coexpressed in BaF3 cells. After incubation with TEV protease to shed the ectodomains, activation was evaluated with STAT5 phosphorylation.

Both WT receptors (hIL-7R and hγc) and cleavable receptors (TEV–hIL-7R and TEV-hγc) were well expressed on the cell membrane with enhanced green fluorescent protein (EGFP) and mCherry fused to the C termini of hIL-7R and hγc, respectively (fig. S1A). Colocalization of hIL-7R and hγc as well as sparse bright puncta were observed in the absence of hIL-7, consistent with previous accounts of both homotypic preassociation of hIL-7R (*21*) and heterotypic preassociation with hγc (*22*, *23*). More puncta appeared on the cell surface after ligand incubation as a result of greater receptor clustering induced by ligand binding. Predictably, this was accompanied by receptor activation as indicated by STAT5 phosphorylation (fig. S1B). The TEV-cleavable hIL-7R and hγc exhibited analogous ligand response to that of the WT receptors (fig. S1B) but could be activated by incubating BaF3 cells with TEV protease in the absence of ligand (Fig. 1C). The TEV protease dose-response profile revealed that ~40% maximal activation could be reached compared with IL-7–induced activation (Fig. 1D) and that the increase of receptor activation correlated with increased shedding of receptor ectodomains from the cell surface (fig. S1, C to H). More cell-surface puncta were observed after treatment with 50 μg/ml of TEV protease, which suggests the ability of TMH-ICD to cluster, though substantially less than in the context of ectodomain-ligand engagement (fig. S1I). By contrast, no activation was detected after adding TEV protease to cells expressing WT receptors (Fig. 1, C to D, and fig. S1I). Similar receptor activity induced by proteolytic removal of ectodomain was observed for cleavable hIL-9R and hγc (fig. S2), which suggests that heterotypic interaction of TMDs is a general phenomenon for γc receptor family members.

To independently examine the functional consequence of ectodomain removal, we

[1]Department of Biological Chemistry and Molecular Pharmacology, Harvard Medical School, Boston, MA 02115, USA. [2]Program in Cellular and Molecular Medicine, Boston Children's Hospital, Boston, MA 02115, USA.
*Corresponding author. Email: james_chou@hms.harvard.edu
†These authors contributed equally to this work.
‡Present address: High Magnetic Field Laboratory, Hefei Institutes of Physical Science, Chinese Academy of Sciences, Science Island, Hefei, 230031, China.
§Present address: Interdisciplinary Research Center on Biology and Chemistry, Shanghai Institute of Organic Chemistry, Chinese Academy of Sciences, Shanghai, 201203, China.

designed two constructs with the ectodomain (ECD) deleted (hIL-7R–ΔECD and hγc-ΔECD) and expressed each of them alone or paired with a WT or ectodomain-deleted receptor (Fig. 1E). The membrane integrations of hIL-7R–ΔECD and hγc-ΔECD were confirmed by confocal microscopy (fig. S1J). Among receptor-expressing cells, those co-expressing hIL-7R–ΔECD and hγc-ΔECD exhibited the strongest signaling, reaching ~40% of ligand-induced STAT5 phosphorylation by the WT receptors (Fig. 1, F and G). This result

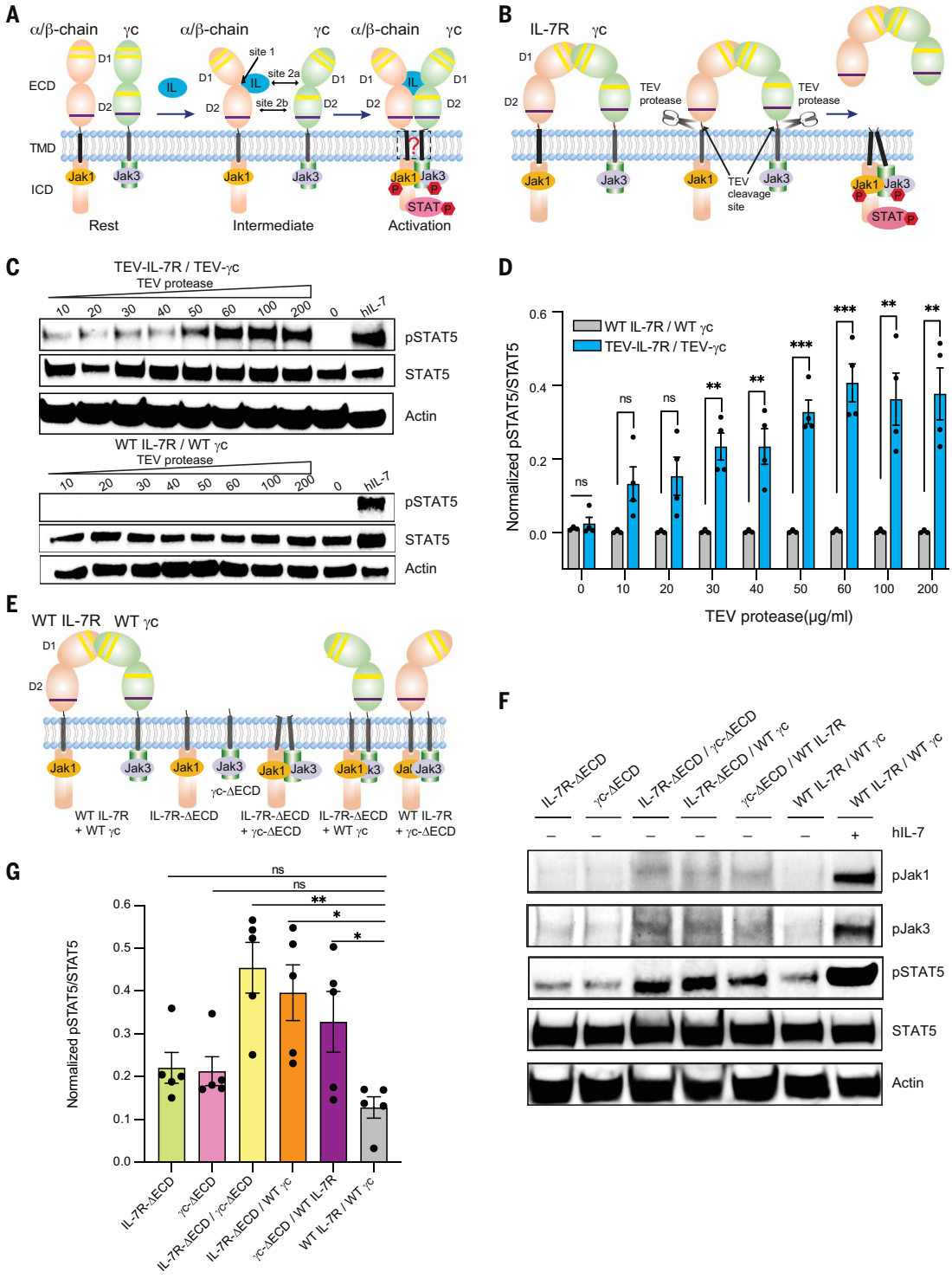

Fig. 1. Removal of the ectodomains of IL-7R and γc activates IL-7R signaling. (**A**) The prevailing model of cytokine-mediated receptor sharing for receptors in the common γc receptor family. Receptors in this family are type I membrane proteins comprising a ligand binding ectodomain (ECD), a TMD, and an ICD with docking sites for the JAK-STAT signaling molecules. (**B**) The autoinhibition hypothesis postulating that preligand association of ECDs hinders clustering of TMD-ICD for activation and that proteolytic removal of the ECDs should allow TMD-driven receptor pairing and cytokine-independent signaling. (**C**) IL-7R pathway activation detected by immunoblotting of STAT5 phosphorylation (pSTAT5) in BaF3 cells coexpressing cleavable receptors (TEV–IL-7R and TEV-γc) (top) or WT receptors (WT IL-7R and WT γc) (bottom) after treatment with 0 to 200 μg/ml of TEV protease or 50 ng/ml of hIL-7. (**D**) Quantification of protease-induced pSTAT5 signals in (C) as pSTAT5/STAT5 intensity ratios, which are further normalized relative to that induced by hIL-7. The data are shown as means ± SEMs calculated from all technical replicates from three independent experiments (with one to two technical replicates per experiment). Statistical significance by Student's *t* test. ns, not significant; $^{**}P \le 0.01$; $^{***}P \le 0.001$. (**E**) Schematic illustration of all possible combinations of full-length receptors (IL-7R, γc) and ECD-deleted receptors (IL-7R–ΔECD, γc-ΔECD) expressed in BaF3 cells for testing ligand-independent signaling. (**F**) IL-7R pathway activation reported by phosphorylation of STAT5, JAK1, and JAK3 in BaF3 cells expressing full-length and ECD-deleted receptor combinations illustrated in (E). (**G**) Quantification of pSTAT5 signals in (F) as pSTAT5/STAT5 intensity ratios, which are further normalized relative to that induced by hIL-7. The data are shown as means ± SEMs calculated from all technical replicates from three independent experiments (with one to two technical replicates per experiment). Statistical significance by Student's *t* test. ns, not significant; $^{*}P \le 0.05$; $^{**}P \le 0.01$.

was consistent with the activation achieved by proteolytic removal of ectodomains (Fig. 1, C and D). The cells expressing hIL-7R–ΔECD or hγc-ΔECD (with a WT receptor) also showed weaker but measurable ligand-independent signaling (Fig. 1, F and G), which suggests that both hIL-7R and hγc ectodomains are involved in receptor autoinhibition in the absence of ligand. They would prevent the TMD-ICD regions of hIL-7R and hγc from forming signaling-competent complexes. Thus, TMDs appear to play an active role in the heterotypic association between hIL-7R and hγc that drives signaling.

TMD interactions match the receptor-sharing network

We next investigated whether the TMD of the γc (designated γcTMD) could directly associate with that of ILR members (designated IL-xRTMD) in the cell membrane and whether the heterodimerization of TMDs also exhibited properties of receptor sharing as do the ectodomains. We selected the TMDs of γc, IL-4R, IL-7R, and IL-9R from both human and mouse to test oligomerization (Fig. 2A). We also selected the TMD of IL-5R from the β chain (βc) family to examine possible nonspecific association with γcTMD. The TMD sequences of these receptors (fig. S3) did not show any conserved small-xxx-small motif that mediates TMH dimerization in growth factor receptors (*16*, *24*–*26*). Nor did they show charged residues that mediate intramembrane assembly of activating immunoreceptors (*27*–*29*). Thus, pairing of the γc TMD with different ILR TMDs was mediated possibly by a previously unrecognized type of interaction.

TMD interactions were examined using a bacterial adenylate cyclase two-hybrid (BACTH) assay (*30*). Briefly, two complementary domains (T18 and T25) of adenylate cyclase (AC) were

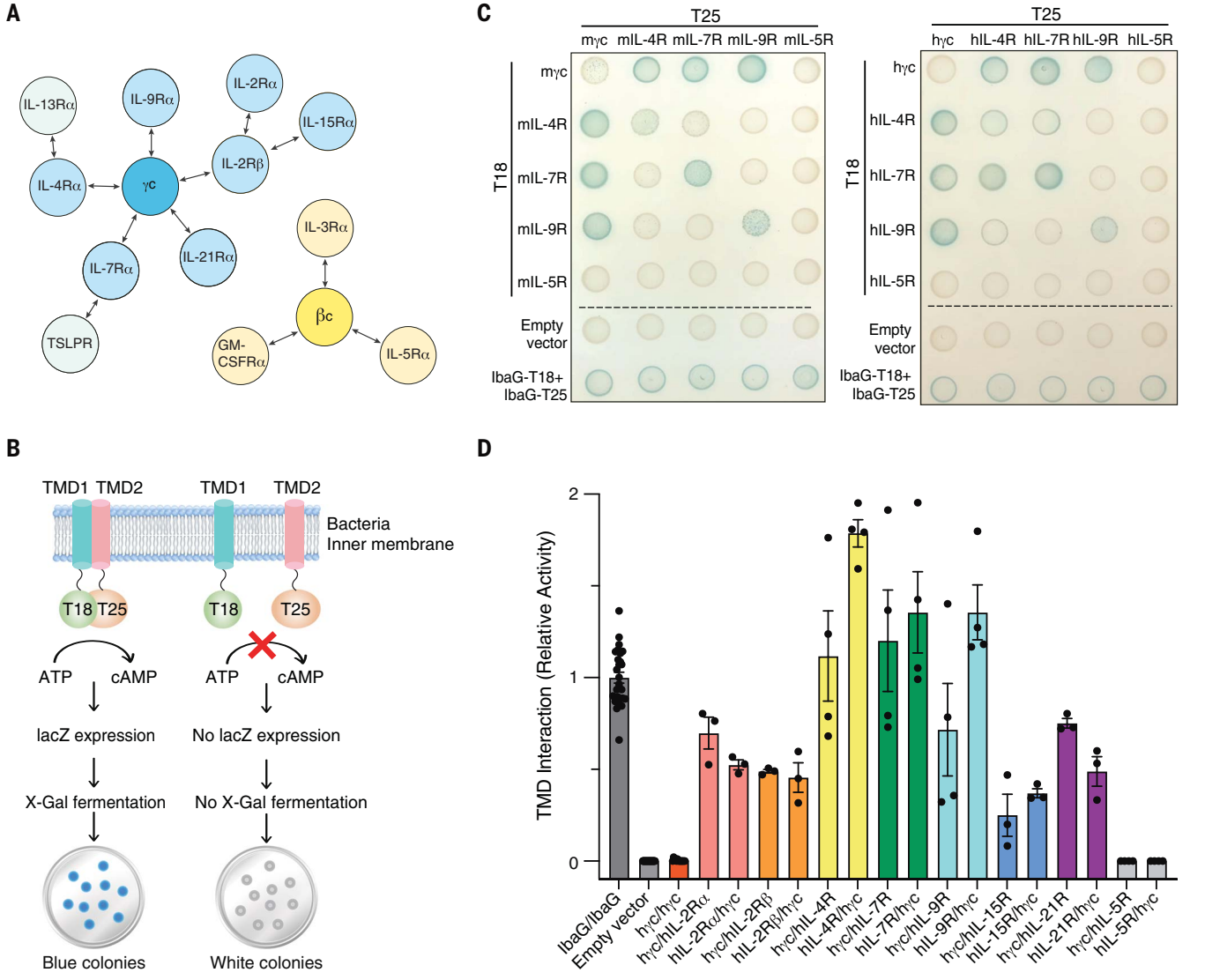

Fig. 2. Specific heterodimerization of γcTMD with the TMDs of its family members. (**A**) Schematic diagram showing receptor-sharing network for the γc (blue) and βc (yellow) receptor families. Some complexes require a third chain for cytokine recognition and signal transduction, such as IL-2Rα and IL15Rα. IL-4Rα and IL-7Rα can also form heterodimer complexes with IL-13Rα and TSLPR, respectively. (**B**) Schematic illustration of the BACTH system (*30*) for analyzing TMD interactions. ATP, adenosine 5′-triphosphate; cAMP, adenosine 3′,5′-monophosphate; lacZ, β-galactosidase; X-Gal, X-galactosidase. (**C**) BACTH analysis of TMD interactions for representative γc family receptors and the βc family member IL-5R from both mice and humans. Blue colonies indicate TMD-TMD association in the bacteria inner membrane. (**D**) Quantification of BACTH colony colors, which are normalized relative to the IbaG/IbaG positive control. The data are shown as means ± SEMs calculated from technical replicates (typically three to four) from one representative of three independent experiments.

fused, separately, to the TMDs under investigation (Fig. 2B). The TMD fusion proteins were expressed in an AC-deficient (CyaA) strain that yielded white bacteria colonies by default. Stable association of two TMDs reconstitutes AC activity, resulting in blue colonies. For both mouse and human sequences, γcTMD can stably heterodimerize with the TMDs of IL-4R, IL-7R, and IL-9R—the corresponding colonies showed the strongest blue colors (Fig. 2C and fig. S4). By contrast, no association between the TMDs of γc and IL-5R was detected (Fig. 2C and fig. S4), which indicates no cross-family TMD association. Additional BACTH results for human γc, IL-2Rα, IL-2Rβ, IL-15R, and IL-21R from the γc family and for human βc and IL-5R from the βc family (fig. S5) demonstrated that heterotypic TMD associations are consistent with the γc family receptor–sharing network (Fig. 2D).

A homotypic TMD interaction was also observed for IL-2Rα and IL-2Rβ, IL-4R, IL-7R, IL-9R, and IL-21R, though on average it was weaker than the heterotypic interaction involving γcTMD (Fig. 2C and fig. S5). Although the function of homotypic TMD interactions is unknown, it may contribute to preassembly of ILRs before ligand engagement. A previous study had suggested that the IL-2Rα and IL-2Rβ are already colocalized in resting T cells in the absence of IL-2 (*31*).

Structures of γcTMD in complex with IL-7RTMD and with IL-9RTMD in bicelles

The specific recognition of the TMDs of γc family ILRs by γcTMD was unexpected because their sequences are highly divergent (fig. S3). To understand the structural basis of receptor sharing at the membrane level, we determined high-resolution nuclear magnetic resonance (NMR) structures of two representative heterodimer complexes in bicelles mimicking a lipid bilayer: γcTMD bound to IL-7RTMD (figs. S6 and S7) and γcTMD bound to IL-9RTMD (figs. S6 and S8). In addition, an intermolecular nuclear Overhauser effect (NOE) difference experiment revealed γcTMD residues in the interaction interface. I274, L277, and I278 in particular experienced intermolecular NOE both in complex with IL-7RTMD and with IL-9RTMD (Fig. 3A).

The two transmembrane heterodimer structures were unexpectedly homologous. Foremost, this structural similarity was characterized by

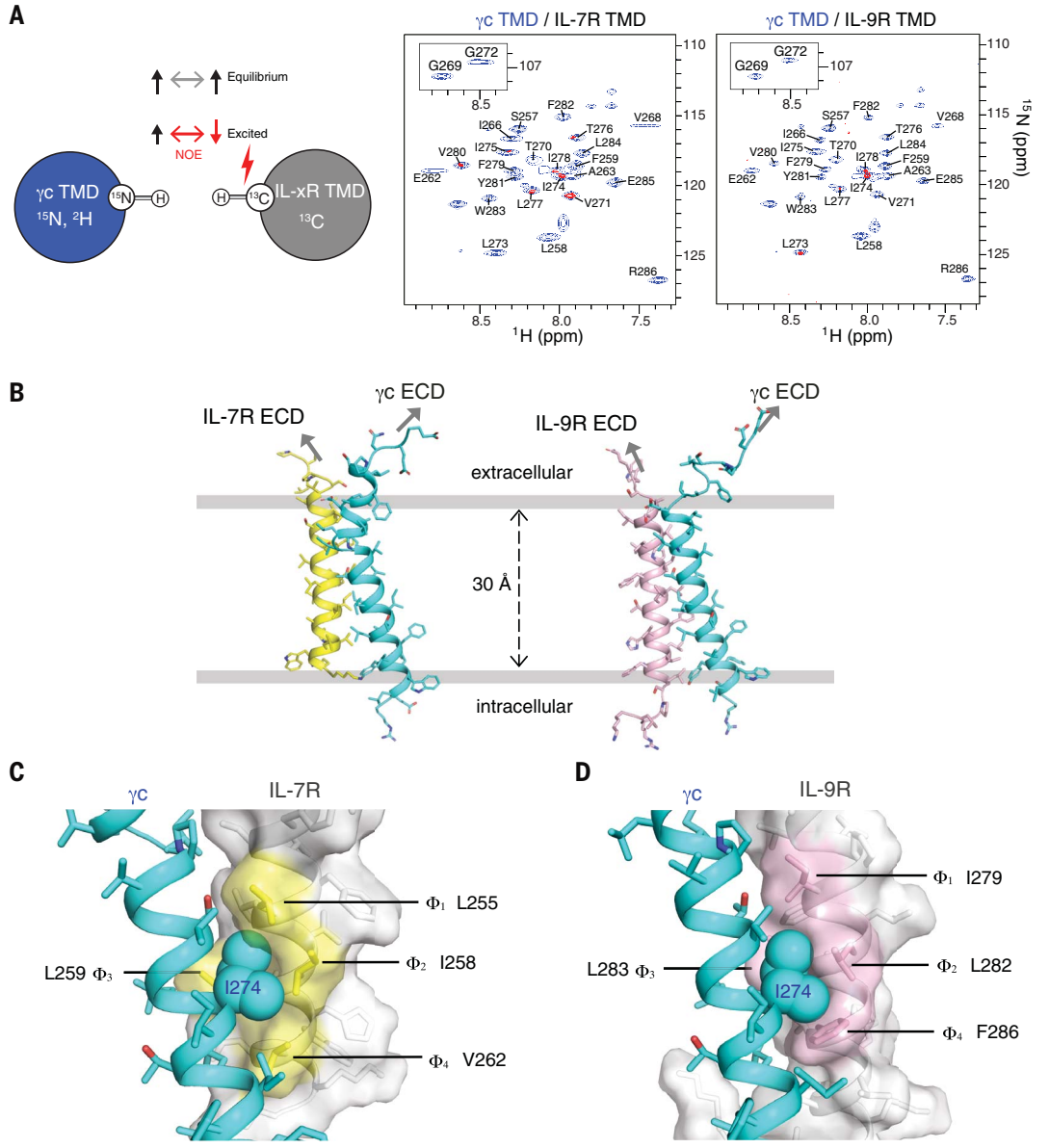

Fig. 3. NMR structures of γcTMD in complex with IL-7RTMD and with IL-9RTMD show a common knob-into-hole mechanism of recognition. (**A**) (Left) Detecting residue-specific interchain NOEs using the sample of (^{15}N, ^{2}H) γcTMD mixed with (^{13}C) IL-7RTMD or IL-9RTMD at a 1:1 molar ratio. The experiment involves recording two interleaved ^{1}H-^{15}N TROSY-HSQC spectra: one at equilibrium and the other with the ^{13}C-attached aliphatic protons inverted during 200 ms of NOE mixing. (Right) Overlaying the difference between two interleaved ^{1}H-^{15}N TROSY-HSQC spectra (red) onto the reference spectrum (blue) reveals γcTMD residues in close contact with IL-7/9RTMD. The spectra were recorded at 303 K and ^{1}H frequency of 900 MHz. ppm, parts per million. (**B**) Ribbon representation of the structures of γcTMD in complex with IL-7RTMD (left) and with IL-9RTMD (right) in DMPC-DH_6PC bicelles with q = 0.4. (**C**) A close-up view of γcTMD I274 (sphere) fitting into the hydrophobic pocket of IL-7RTMD (yellow) formed by the Φ_1-xx-$\Phi_2\Phi_3$-xx-Φ motif. (**D**) The same close-up view as in (C) of γcTMD I274 fitting into the pocket of IL-9RTMD (pink). Single-letter abbreviations for the amino acid residues are as follows: A, Ala; C, Cys; D, Asp; E, Glu; F, Phe; G, Gly; H, His; I, Ile; K, Lys; L, Leu; M, Met; N, Asn; P, Pro; Q, Gln; R, Arg; S, Ser; T, Thr; V, Val; W, Trp; and Y, Tyr.

an ~20° helical packing angle and the involvement of the same face of γcTMD in packing against IL-7RTMD or IL-9RTMD (IL-7/9RTMD) (Fig. 3B). Closer inspection of the two structures identified I274 of γcTMD as the key residue that filled a hydrophobic hole of IL-7/9RTMD comprising four residues (Fig. 3, C and D), reminiscent of a knob-into-hole mechanism. These four residues had a sequence arrangement of Φ_1-xx-$\Phi_2\Phi_3$-xx-Φ_4, where Φ_i represents hydrophobic residues such as isoleucine, leucine, valine, and phenylalanine that constitute the pocket. Other γcTMD residues, I266, P267, T270, and L277 also made close van der Waals (VDW) contacts with receptor TMDs but did not appear to be locked into a hole (Fig. 4, A and B). For the receptor TMD, S252, L255, L259, and V262 of IL-7RTMD and I279, L282, L283, and F286 of IL-9RTMD were in close VDW contact with γcTMD, but none of them were wrapped by a defined pocket (Fig. 4, A and B).

Mutating P267, T270, I274, or L277 of γcTMD to tyrosine disrupted heterodimerization with IL-4RTMD, IL-7RTMD, and IL-9RTMD (Fig. 4C and fig. S9, A to H). A similar pattern was observed for IL-21RTMD (fig. S9I). Mutating S252 or L255 of IL-7RTMD to tyrosine also abolished heterodimerization (Fig. 4D and fig. S9J). Thus, these NMR structures are consistent with those expressed in the cell membrane and reveal that intramembrane recognition by the γc of different family members is based largely on the same knob-into-hole mechanism (Fig. 4E).

This relatively small binding area—501.4 Å^2 between γcTMD and IL-7RTMD or 479.0 Å^2 between γcTMD and IL-9RTMD—was consistent with the small number of residues involved in the knob-into-hole interaction. Confinement of interaction to a small area could explain why IL-7RTMD and IL-9RTMD could both be recognized by γcTMD despite only having 35% identity. This interaction is reminiscent of the small interaction interface between the γc ectodomain and cytokines (7), which suggests that degenerate recognition by the γc is possible because of a small but structurally consistent recognition surface pattern.

Essential role of the knob-into-hole interaction in the membrane for IL-7R signaling

To determine whether the specific knob-into-hole mechanism of TMD heterodimerization is relevant to receptor signaling, we performed

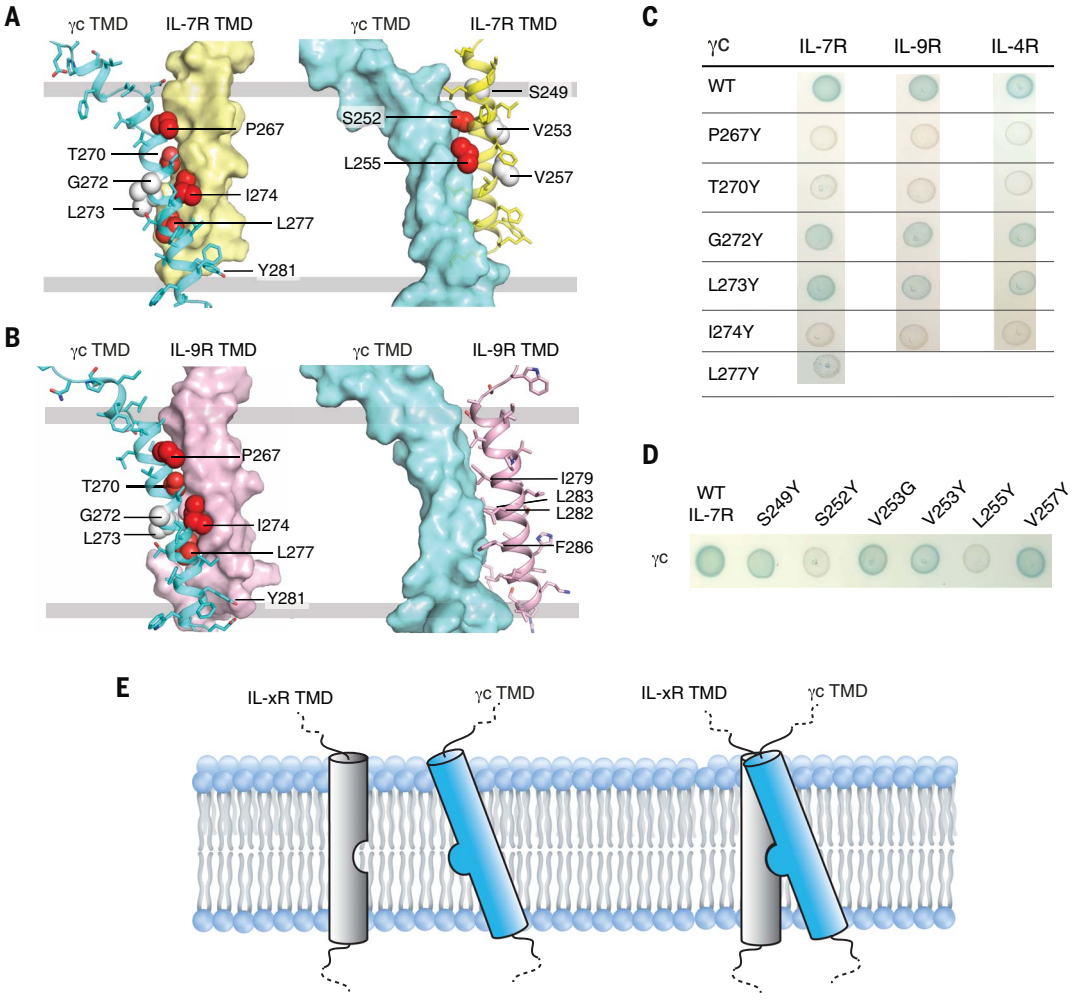

Fig. 4. Validation of the surface complementarity and the common mechanism of γcTMD sharing by mutagenesis. (**A**) The contours of the γcTMD–IL-7RTMD heterodimer interface shown with the IL-7RTMD strand surface rendered (left) and the γcTMD surface rendered (right). The γcTMD and IL-7RTMD residues in sphere are residues tested by mutagenesis in (C), with red and white indicating dimer disruption and no effect, respectively. (**B**) Same as in (A) for the γcTMD–IL-9RTMD heterodimer. (**C**) BACTH analysis of the effect of γcTMD mutations on γcTMD association with IL-7RTMD, IL-9RTMD, or IL-4RTMD. Corresponding mutations for human sequences are shown in fig. S9. Results are from one representative of three independent experiments with three replicates per experiment. (**D**) BACTH analysis of the effect of IL-7RTMD mutations on association with γcTMD. Results are from one representative of three independent experiments with three replicates per experiment. (**E**) Schematic illustration of the knob-into-hole mechanism of recognition that mediates receptor sharing within the membrane.

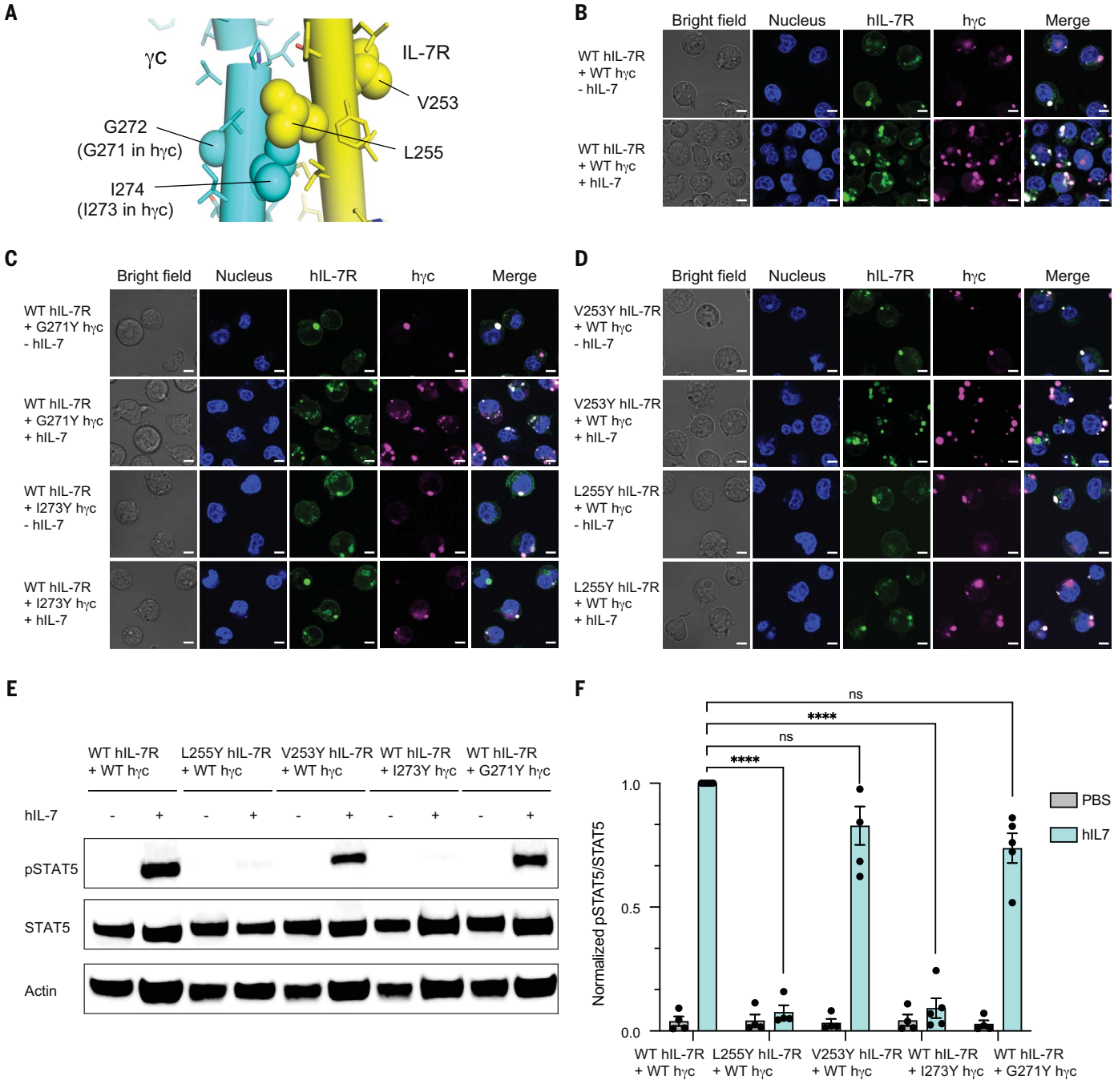

Fig. 5. Specific TMD heterodimerization is required for ligand-induced IL-7R signaling. (**A**) Cylinder representation of the γcTMD–IL-7RTMD heterodimer structure showing the positions of the TMD residues of γc and IL-7R (sphere) that were tested for ligand-induced receptor signaling. Specifically, I274 of γcTMD and L255 of IL-7R are important for the knob-into-hole mechanism, whereas G272 of γcTMD and V253 of IL-7R are not involved in heterodimerization. (**B** to **D**) Coexpression and distribution of WT hIL-7R (green) and hγc (magenta), of WT hIL-7R (green) and hγc mutants (magenta), and of WT hγc (magenta) and hIL-7R mutants (green) on the surface of BaF3 without and with treatment with hIL-7. The nuclei of 1×10^6 cells were stained with 4′,6-diamidino-2-phenylindole (DAPI) (blue). Three independent experiments were performed with two replicates per experiment. The images represent one of two biological replicates with similar results. Scale bars, 5 μm. (**E**) Phosphorylation of STAT5 (pSTAT5) in BaF3 cells coexpressing WT or mutant hIL-7R with WT or mutant hγc after treatment with 50 ng/ml of hIL-7. The pSTAT5 signals were detected by immunoblotting (top) and compared with immunoblot signals of STAT5 (middle). (**F**) Quantification of pSTAT5 signals in (E) as pSTAT5/STAT5 intensity ratios, normalized relative to that of the WT receptors. The data are shown as means ± SEMs calculated from all technical replicates from three independent experiments (with one to two technical replicates per experiment). Statistical significance by Student's *t* test. ns, not significant; ****$P \leq 0.0001$. PBS, phosphate-buffered saline.

structure-guided mutagenesis and tested these mutants using functional assays similar to those used for receptor activation by TEV protease (Fig. 1, C and D). On the basis of the structure of γcTMD in complex with IL-7RTMD, the knob residue of γcTMD was I274 in mice and I273 in humans, and a key constituent of the hole in IL-7RTMD is L255 (Fig. 5A). These residues were mutated to tyrosine to disrupt the knob-into-hole interaction. In addition, the glycine on the opposite side of the γcTMD (G271 in humans) and V253 on the opposite side of the IL-7RTMD were mutated to tyrosine as no-effect mutations.

Full-length hγc and hIL-7R as well as their single mutants were expressed in BaF3 cells. The surface expressions of the mutants were all within ~28% of that of the WT (fig. S10) and exhibited similar levels of hIL-7 binding (fig. S11). Sparse puncta were observed before ligand addition for all variants, which suggests that the introduction of the TMD mutations did not affect preligand association (Fig. 5, B to D). Many more puncta appeared after ligand addition for cells coexpressing WT hIL-7R and G271Y hγc and for cells coexpressing V253Y hIL-7R and WT hγc (Fig. 5, C and D), consistent with IL-7–induced receptor clustering. By contrast, cells expressing either I273Y hγc or L255Y hIL-7R showed no detectable increase of puncta after ligand addition, which indicates that preventing TMD heterodimerization reduced ligand-induced receptor clustering.

The imaging results were independently confirmed by immunoblot analysis of STAT5 phosphorylation. Disrupting either the knob with the I273Y mutation or the hole with the L255Y mutation completely abolished signaling, whereas G271Y in hγc or V253Y in hIL-7R showed no detectable differences in signaling compared with the WT receptors (Fig. 5, E and F). Similarly, a mutation of IL-9R that disrupts TMD heterodimerization (L282Y) also abolished signaling, whereas a mutation away from the heterodimer interface (T284Y) showed no effect on signaling (fig. S12). Thus, the heterotypic association of receptor TMDs mediated by the knob-into-hole mechanism is essential for ligand-induced signaling of IL-7R and IL-9R. Moreover, this mechanism is likely applicable to other members of the γc family.

Although the V253Y mutation of IL-7RTMD did not alter signaling, consistent with the structure, the gain-of-function mutation V253G (*18*) could mediate a homotypic IL-7RTMD interaction that enhanced receptor clustering and signaling, as glycine is often implicated in TMH dimerization. In addition to knob-into-hole interaction mutations, we tested hγc TMD mutations found in patients with severe combined immunodeficiency diseases (SCIDs), including I265N, G268R, M270R, G271E, C278W, and V279M (*32*–*34*) (fig. S13). These results are consistent with the finding that TMD heterodimerization is required for signaling. The mutations C278W and V279M did not significantly reduce TMD heterodimerization between γc and IL-7R– or IL-7–induced signaling (fig. S13, F and H). However, these mutations may affect γc intramembrane interaction in the more complicated trimeric complex comprising IL-2Rα or IL-15Rα, IL-2Rβ, and γc TMDs (Fig. 2A).

Discussion

The γc TMD is capable of specific recognition of multiple ILR TMDs that have low sequence homology (fig. S3). A notable structural question is how specificity and promiscuity are concomitantly achieved. The complementary surface representations of IL-7/9RTMD and γcTMD (Fig. 3) show that IL-7RTMD and IL-9RTMD both have a deep pocket fitting the I274 knob of γcTMD. In this context, the I274 knob of γcTMD can be perceived as the key that fits the small hydrophobic hole (or lock) presented by the different ILR TMDs, which would explain the promiscuity. The structural features governing specificity, however, may go beyond the knob-into-hole module. The vertical positions in the lipid bilayer of the two TMDs are important for aligning the I274 knob with the hydrophobic hole for binding. Other supporting interactions may further enhance specificity, such as the interaction of L277 and Y281 of γcTMD with the complementary surface of the receptor TMD near its C-terminal end (Fig. 4, A and B). The three γcTMD residues with 100% conservation across species (I274, L277, and Y281) (fig. S3) are precisely those residues making close VDW contacts with the receptor TMDs in our structures.

Specific TMD pairing required for signaling of the γc family receptors may inform the generation of TMDs that can modulate receptor activity. Although the design of transmembrane proteins remains challenging, several studies have demonstrated its feasibility for TMD oligomerization (*35*–*37*). The use of a designed transmembrane peptide to modulate immunoreceptor activity by competing with the TMD heterodimerization between the integrin α and β subunits could push the equilibrium from an inactive to an active state (*38*). More recently, designed TMD oligomerization has been applied to mediate chimeric antigen receptor (CAR) oligomerization to enhance the therapeutic window of CAR T immunotherapies (*39*). The distinct features of the knob-into-hole interaction that mediate γc sharing and the structural differences among the ILR members of the family could be exploited to fashion decoy γcTMDs for the selective interference of cytokine signaling.

The partial signaling after removal of receptor ectodomains strongly suggests that they are arranged in an autoinhibitory state in the absence of ligand. This autoinhibition likely involves homotypic and heterotypic associations of the ectodomains of ILRs and γc, which is consistent with our observation that the coexpression of IL-7R and γc resulted in their colocalization on the cell surface (fig. S1, A and I). The preligand association of ILRs and γc may also organize the receptors for a biased response to ligand activation. Previous studies have shown that preassociation of the γc with the IL-7R reduces the amount of free γc for other members of the family, which results in asymmetrical cross-talk toward stimulation with different cytokines (*22*, *23*). To date, no structural information has been made available for heterotypic preligand association in the γc receptor family. A crystal structure of homotypic association, however, has been reported for the IL-7R ectodomain (*21*), which shows a head-to-head antiparallel configuration proposed to be autoinhibitory, as it keeps the TMD-ICDs apart (*19*).

It is unclear whether the TMD homotypic interaction competes or synergizes with the heterotypic TMD interaction in receptor activation. Our intermolecular NOE data of IL-7RTMD in bicelles suggest that TMD self-association is driven by the packing of hydrophobic residues (F251, L255, and I258) from the opposite TMDs (fig. S14, A and B). The L255Y mutation prevented hIL-7RTMD self-association in the BACTH assay (fig. S14C), but L255 is an integral part of the hydrophobic pocket in the knob-into-hole mechanism (Fig. 3C). Thus, at least in the case of IL-7RTMD, the homotypic association is expected to compete with the heterotypic interaction with the γc TMD. The functional relevance of this result remains to be studied.

We have demonstrated that TMDs of the γc family of cytokine receptors can conserve specificity without sacrificing promiscuity using a knob-into-hole recognition pattern that mediates receptor sharing in the membrane and is important for receptor activation. Our finding provides a conceptual framework for constructing TMHs to modulate γc family receptor activities to potentially address the gain- or loss-of-function disease mutations associated with these TMDs.

REFERENCES AND NOTES

1. W. J. Leonard, *Nat. Rev. Immunol.* **1**, 200–208 (2001).
2. Y. Rochman, R. Spolski, W. J. Leonard, *Nat. Rev. Immunol.* **9**, 480–490 (2009).
3. R. Spolski, W. J. Leonard, *Annu. Rev. Immunol.* **26**, 57–79 (2008).
4. J.-X. Lin, W. J. Leonard, *Cold Spring Harb. Perspect. Biol.* **10**, a028449 (2018).
5. W. J. Leonard, J. X. Lin, J. J. O'Shea, *Immunity* **50**, 832–850 (2019).
6. X. Wang, M. Rickert, K. C. Garcia, *Science* **310**, 1159–1163 (2005).
7. X. Wang, P. Lupardus, S. L. Laporte, K. C. Garcia, *Annu. Rev. Immunol.* **27**, 29–60 (2009).
8. S. L. LaPorte *et al.*, *Cell* **132**, 259–272 (2008).

9. K. F. Kubatzky *et al*., *Curr. Biol.* **11**, 110–115 (2001).
10. E. E. Matthews *et al*., *FASEB J.* **25**, 2234–2244 (2011).
11. N. Yang, X. Wang, J. Jiang, S. J. Frank, *Mol. Endocrinol.* **21**, 1642–1655 (2007).
12. E. V. Bocharov *et al*., *Biochim. Biophys. Acta Gen. Subj.* **1862**, 1410–1420 (2018).
13. Q. Fu *et al*., *Mol. Cell* **61**, 602–613 (2016).
14. L. Pan *et al*., *Cell* **176**, 1477–1489.e14 (2019).
15. A. Arkhipov *et al*., *Cell* **152**, 557–569 (2013).
16. N. F. Endres *et al*., *Cell* **152**, 543–556 (2013).
17. G. Skiniotis, P. J. Lupardus, M. Martick, T. Walz, K. C. Garcia, *Mol. Cell* **31**, 737–748 (2008).
18. C. Shochat *et al*., *Blood* **124**, 106–110 (2014).
19. S. T. Walsh, *Immunol. Rev.* **250**, 303–316 (2012).
20. G. Du *et al*., *Cell Res.* **33**, 131–146 (2023).
21. C. A. McElroy *et al*., *Proc. Natl. Acad. Sci. U.S.A.* **109**, 2503–2508 (2012).
22. P. Gonnord *et al*., *Sci. Signal.* **11**, eaal1253 (2018).
23. A. T. Waickman *et al*., *iScience* **23**, 101421 (2020).
24. K. R. MacKenzie, J. H. Prestegard, D. M. Engelman, *Science* **276**, 131–133 (1997).
25. E. V. Bocharov *et al*., *J. Biol. Chem.* **283**, 6950–6956 (2008).
26. R. Trenker, M. E. Call, M. J. Call, *J. Am. Chem. Soc.* **137**, 15676–15679 (2015).
27. M. E. Call, K. W. Wucherpfennig, *Nat. Rev. Immunol.* **7**, 841–850 (2007).
28. M. E. Call, K. W. Wucherpfennig, J. J. Chou, *Nat. Immunol.* **11**, 1023–1029 (2010).
29. L. K. Fong, M. J. Chalkley, S. K. Tan, M. Grabe, W. F. DeGrado, *Proc. Natl. Acad. Sci. U.S.A.* **118**, e2026318118 (2021).
30. A. Battesti, E. Bouveret, *Methods* **58**, 325–334 (2012).
31. S. Damjanovich *et al*., *Proc. Natl. Acad. Sci. U.S.A.* **94**, 13134–13139 (1997).
32. J. M. Puck *et al*., *Blood* **89**, 1968–1977 (1997).
33. J. E. Niemela, J. M. Puck, R. E. Fischer, T. A. Fleisher, A. P. Hsu, *Clin. Immunol.* **95**, 33–38 (2000).
34. C. M. Yao *et al*., *J. Clin. Immunol.* **33**, 526–539 (2013).
35. I. V. Korendovych, W. F. DeGrado, *Q. Rev. Biophys.* **53**, e3 (2020).
36. P. Lu *et al*., *Science* **359**, 1042–1046 (2018).
37. P. Barth, A. Senes, *Nat. Struct. Mol. Biol.* **23**, 475–480 (2016).
38. H. Yin *et al*., *Science* **315**, 1817–1822 (2007).
39. A. Elazar *et al*., *eLife* **11**, e75660 (2022).

ACKNOWLEDGMENTS

We thank Q. Fu and W. Chen for their help with protein biochemistry, A. Zoued and R. Ian for sharing materials for the BACTH assay, and J. Li for their technical support of virus packaging. We thank C. Xie and S. Blacklow for their insightful discussions. **Funding:** This work was supported by NIH grants GM140887 (to J.J.C.) and AI150709 (to J.J.C. and H.W.). The NMR data were collected at the MIT-Harvard Center for Magnetic Resonance (supported by NIH grants P41 GM132079 and S10 OD023513). **Author contributions:** T.C., R.L.C., H.W., and J.J.C. conceived the study. T.C. and R.L.C. prepared samples and performed NMR analyses. T.C. and R.L.C. performed the BACTH assays. T.C. performed functional cell assays. X.P. assisted with cell assays. J.J.C., T.C., and R.L.C. wrote the paper, and the other authors helped with editing the paper. **Competing interests:** The authors declare no competing interests. **Data and materials availability:** The atomic structure coordinate and structural constraints have been deposited in the Protein Data Bank (PDB) with accession numbers 8DDC (γcTMD–IL-7RTMD) and 8DDD (γcTMD–IL-9RTMD). The chemical shift values have been deposited in the Biological Magnetic Resonance Data Bank (BMRB) with accession numbers 31026 (γcTMD–IL-7RTMD) and 31027 (γcTMD–IL-9RTMD). All data are available in the main text or the supplementary materials.

SUPPLEMENTARY MATERIALS

science.org/doi/10.1126/science.add1219
Materials and Methods
Figs. S1 to S14
Tables S1 and S2
References (*40*–*53*)
MDAR Reproducibility Checklist

Submitted 22 May 2022; resubmitted 25 October 2022
Accepted 23 June 2023
10.1126/science.add1219

Structural basis of # chain family receptor sharing at the membrane level

Tiantian Cai, Rachel Lenoir Capello, Xiong Pi, Hao Wu, and James J. Chou

Science, **381** (6657), .
DOI: 10.1126/science.add1219

Editor's summary
Gamma-chain (#c) cytokine receptors play critical roles in the development, proliferation, and activation of immune cells. They are composed of a common #-chain that associates with interleukin receptor (ILR) subunits specific to each cytokine. Association between these subunits is driven by interleukin binding to ILR ectodomains and subsequent recruitment of the #c. Cai *et al*. used nuclear magnetic resonance spectroscopy and functional mutagenesis of two ILRs to show that the transmembrane domains, which link ectodomains to intracellular signaling domains, also play an active role in signaling. The authors further show that the #c transmembrane domain can specifically recognize various ILR transmembrane domains from the #c receptor family through a conserved "knob-into-hole" mechanism. —Seth Thomas Scanlon

Science
AAAS

Supplementary Materials for

Structural basis of γ chain family receptor sharing at the membrane level

Tiantian Cai *et al*.

Corresponding author: James J. Chou, james_chou@hms.harvard.edu

Science **381**, 569 (2023)
DOI: 10.1126/science.add1219

The PDF file includes:

Other Supplementary Material for this manuscript includes the following:

Materials and Methods

Cell lines

BaF3 cell line

Cytokine-dependent BaF3 cells were cultured in RPMI 1640 (GIBCO, ThermoFisher Scientific) medium supplemented with 10% fetal bovine serum (GIBCO, ThermoFisher Scientific), 10 ng/ml of mouse interleukin-3 (mIL-3) (Sigma) and 100 U/ml of pen–strep (GIBCO, ThermoFisher Scientific) at 37°C, 5% CO_2.

HEK293T cell line

Human kidney epithelial cell line HEK293T cells (ATCC# CRL-3216; RRID: CVCL_0063) were purchased from ATCC. HEK293T cells were maintained in DMEM (GIBCO, ThermoFisher Scientific) supplemented with 10% fetal bovine serum (GIBCO, ThermoFisher Scientific) and 100 U/ml of pen–strep (GIBCO, ThermoFisher Scientific) at 37°C, 5% CO_2.

Bacterial two-hybrid (BACTH) expression and interaction assay

A bacterial two-hybrid (BACTH) system based on the reconstituted activity of adenylate cyclase (AC) (*30*) was adopted to address interaction between transmembrane domains (TMDs) in cell membrane. The BACTH kit (Euromedex, EUK001) was originally purchased from Euromedex and kindly provided by Dr. A. Zoued and R. Ian at Harvard Medical School. To detect TMD interaction, two complementary domains (T18 and T25) of the adenylate cyclase (AC) were fused separately to the C-termini of two TMDs under investigation and the outer membrane protein A (OmpA) was fused to the TMD N-termini for membrane localization. Two plasmids (OmpA-TMD_1-T18, with ampicillin resistance, and OmpA-TMD_2-T25, with kanamycin resistance) encoding the T18 and T25 fusion proteins were transformed into the CyaA deficient *Escherichia coli* strain BTH101. The cotransformed colonies were selected on LB agar plates containing 50 μg/ml of kanamycin and 100 μg/ml of ampicillin after incubation at 30°C for 48 hours. Three colonies for each transformation were selected and cultured in 3 ml of LB medium supplemented with 100 μg/ml of ampicillin, 50 μg/ml of kanamycin and 0.5 mM of IPTG. After overnight growth of the cultures at 30°C with shaking at 220 rpm, 2 μl from each culture was added to the reporter

LB-X-GAL plates containing 40 μg/ml of X-Gal, 100 of μg/ml ampicillin, 50 μg/ml of kanamycin, and 0.5 mM of IPTG. The plates were incubated at 30°C for 24 hours. BolA-like protein IbaG fused with T18 and T25 (IbaG-T18/IbaG-T25), was used as a positive control as previously described (*40*). Coexpression of the empty vector T18 with T25 was used as a negative control. Quantification of BACTH colony color was performed using ImageJ (*41*). The values were normalized relative to that of the IbaG/IbaG positive control. Results are from at least three independent experiments and expressed as mean ± SEM.

Retroviral production and infection of BaF3 cells

Wild-type (WT) or mutants of full-length human IL-7R (hIL-7R) and full-length human IL-9R (hIL-9R) were cloned into retroviral vector MSCV-EGFP with the fusion expression of EGFP at the C-terminus. WT or mutants of full-length human γc (hγc) were cloned into retroviral vector MSCV-mCherry with the fusion expression of mCherry at the C-terminus. Plasmids with single site mutations (V253Y and L255Y of hIL-7R; L282Y and T284Y of hIL-9R; and G271Y, I273Y, I265N, G268R, M270R, I274T, C278W, and V279M of hγc) were generated by site-directed mutagenesis. All constructs were confirmed by DNA sequencing. Retroviral production and transduction were performed as described previously (*42*). HEK293T cells were seeded in 10 cm dishes and cultured until well attached and 60 to 70% confluent. Ten micrograms of retroviral expression plasmid (MSCV- hIL-7R -EGFP or MSCV- hIL-9R -EGFP or MSCV- hγc-mCherry) and 8 μg of packaging helper plasmid pCL-Eco (Addgene, #12371, Cambridge MA) were cotransfected with Lipofectamine 3000 (ThermoFisher Scientific), following the manufacturer's instructions. Twelve hours after transfection, the medium was replaced with fresh DMEM supplemented with 10% FBS. Twenty-four hours after changing the medium (36 hours post transfection), the virus containing supernatant was centrifuged at 1000*g* for 10 min at 4°C to remove cells and debris and filtered through a 0.45-μm sterile filter. The retrovirus was then concentrated with Retro-X Concentrator according to the manufacturer's instructions.

Next, 100 μl of concentrated retroviral supernatant supplemented with 8 μg/ml of polybrene and 10 ng/ml of mIL-3 was used to infect 250,000 BaF3 cells. After overnight incubation at 37°C, the medium was replaced with fresh RPMI1640 supplemented with 2 ml of 10% FBS, 10 ng/ml of mIL-3, 100 U/ml of penicillin, and 100 μg/ml of streptomycin. The infected BaF3 cells were

cultured until they reached a concentration of 2×10^6 cells/ml in 10 ml of medium. To generate the stable cell line, the coexpressing hIL-7R and hγc cells or coexpressing hIL-9R and hγc or single receptor expressing cells were sorted by flow cytometry (Sony SH800Z Cell Sorter) according to the receptor fused EGFP and/or mCherry tags.

Flow cytometry analysis of cell surface expression of receptors

BaF3 cells stably coexpressing WT or mutated human IL-7R and γc were collected and washed twice with fluorescence-activated cell sorting (FACS) buffer (PBS with 1% FBS) and stained for 20 min using 5 μg/ml of Pacific Blue-conjugated anti-hIL-7R antibody (A019D5, BioLegend #351306) and 5 μg/ml of APC-conjugated anti-hγc antibody (TUGh4, BioLegend #338608) on ice. For detecting the co-expression of human WT IL-7R with human γc potential disease mutants (I265N, G268R, M270R, I274T, C278W, and V279M), the cells were stained for 1 hour using 5 μg/ml of Pacific Blue-conjugated anti-hIL-7R antibody (A019D5, BioLegend #351306) and 5 μg/ml of APC-conjugated anti-hγc antibody (TUGh4, BioLegend #338608) on ice. Untransfected BaF3 cells were used as a negative control. After staining, cells were washed twice with the FACS buffer and analyzed for protein expression by flow cytometry (BD, FACSAria 594). Data were analyzed using FCS Express 7 software.

Flow cytometry analysis of cytokine binding to receptors

Human IL-7 binding to WT or mutant receptors was measured using the anti-IL-7 antibody as described previously (*43*). BaF3 cells coexpressing WT hIL-7R and WT hγc or their mutants were collected and washed twice with fluorescence activated cell sorting buffer, followed by incubation with 50 ng/ml of hIL-7 on ice for 30 min. The cells were then fixed with 2% PFA/PBS, immunostained with 5 μg/ml of anti-IL-7 monoclonal antibody (clone ZY335; AbboMax, #604-760) and 5 μg/ml of APC-conjugated anti-rat IgG (H+L) (Invitrogen, #A10540), and analyzed by flow cytometry (BD, FACSAria 594). Untransfected cells were used as control. The experiment was repeated twice. Data were analyzed using FCS Express 7 software.

Cytokine-induced activation

Untransfected (Empty) BaF3 cells and BaF3 stable cell lines coexpressing WT or mutant receptor pairs (hIL-7R or hIL-9R paired with hγc) or receptor pairs with TEV protease site (TEV-hIL-7R

or TEV-hIL-9R with TEV-hγc) were washed three times with PBS followed by cytokine withdrawal by culturing cells without cytokine for 5 hours. After starvation, the cells were stimulated with 50 ng/ml of mIL-3, 50 ng/ml of hIL-7, or 50 ng/ml of hIL-9 in 2 ml of medium in six-well plates for 2 hours at 37°C and then harvested for immunoblot detection.

Activation by proteolytic removal of ectodomain

To test the activation of the IL-7R or IL-9R (IL-7R/9R) pathway by proteolytic removal of the ectodomains (ECDs) of IL-7R/9R and γc without ligand, a TEV protease cleavage sequence (ENLYFQGGGGGS) was introduced between the ECD and TMD for both hIL-7R/9R (TEV-hIL-7R/9R) and hγc (TEV-hγc). Specifically, the insertion was between residues 235 and 236 of hIL-7R (isoform 1) and between residues 251 and 252 of hγc (isoform 1). For IL-9R, the cleavage sequence was between residues 264 and 265. BaF3 stable cell lines co-expressing TEV-hIL-7R/9R and TEV-hγc or coexpressing WT hIL-7R/9R and hγc were generated with retroviral infection as described above. The cells were washed three times with PBS and cultured without cytokine for 5 hours. After cytokine withdrawal, untransfected (empty) BaF3 cells, BaF3 cells expressing WT receptors (hIL-7R/9T and hγc) or receptors cleavable by TEV protease (TEV-hIL-7R/9R and TEV-hγc) were treated with 0, 10, 20, 30, 40, 50, 60, 100 or 200 μg/ml of TEV enzyme in 2 ml of medium in six-well plates overnight at 37°C. The cells were then harvested and the activation of the IL-7R/9R signaling pathway was evaluated by immunoblotting of phosphorylation of STAT5. Results were from three independent experiments with 1-2 technical replicates per experiment and the data points were reported as mean ± SEM of all the technical replicates. Removal of ectodomains of hIL-7R and hγc was confirmed by FACS. BaF3 cells coexpressing TEV-hIL-7R and TEV-hγc were collected after treatment with different concentrations of TEV. Cells were fixed with 2% PFA and washed twice with PBS and stained with 5 μg/ml of Pacific blue-conjugated anti-hIL-7R antibody (A019D5, BioLegend #351306) and 5 μg/ml of APC-conjugated anti-hγc antibody (TUGh4, BioLegend #338608) for 1 hour on ice. After staining, cells were washed twice with FACS buffer and analyzed for receptor ectodomain presentation on cell surface by flow cytometry (BD, FACSAria 594).

Activation due to ectodomain deletion

The hIL-7R with ECD (residues 24 to 235) deleted (hIL-7R-ΔECD) and the hγc with ECD (residues 26 to 251) deleted (hγc-ΔECD) were subcloned into MSCV-EGFP and MSCV-mCherry retroviral vectors, respectively. Retroviral production and infection were performed as described above. BaF3 stable cell lines expressing hIL-7R-ΔECD or hγc-ΔECD (alone or with a WT receptor) were washed three times with PBS followed by cytokine withdrawal by culturing cells without cytokine overnight. The cells were then harvested for immunoblot detection.

Cell imaging

BaF3 stable cell lines expressing the WT, mutant, or ECD-deleted hIL-7R and hγc receptors were washed three times with PBS followed by cytokine withdrawal by culturing cells without cytokine for 5 hours. Observation of receptors without and with cytokine stimulation was undertaken by stimulating cells with either PBS or 50 ng/ml of hIL-7 in 2 ml of medium for 2 hours. For observation of receptor activation by TEV protease, cells were incubated with either PBS, PBS with 50 ng/ml of human hIL-7 or PBS with 50 μg/ml of TEV enzyme overnight at 37 °C. All the cells were transferred to glass-bottomed dishes (ibidi) coated with poly-Lysine and stained with 5 μM of DAPI for 1 hour before imaging. All the images were taken with the Olympus Fluoview FV1000 confocal microscope imaging system equipped with a 60X water objective (Olympus, UPlanApo 60XW, NA=1.2) and read with FV10-ASW 4.2 software.

Immunoblotting

Immunoblotting was used to detect the phosphorylation of STAT5 as described previously (*44*). The harvested cells were washed twice with ice-cold PBS and lysed for 20 min in ice-cold RIPA lysis and extraction buffers supplemented with Halt protease inhibitor cocktail and Halt phosphatase inhibitor cocktail (ThermoFisher Scientific), respectively. The lysates were centrifuged at 18,000 g for 20 min at 4 °C. The supernatants were transferred to clean tubes and NuPAGE LDS Sample Buffer (4X) (ThermoFisher Scientific) was added. After incubation at 95°C for 5 min, the supernatants were subject to 4 to 12% SDS-PAGE (Genscript) and transferred to PVDF membranes (Thermo Scientific). The PVDF membranes were then blocked with 5% BSA in TBS-Tween buffer (20 mM Tris, 150 mM NaCl, 0.1% Tween 20, pH 7.6) overnight at 4°C, followed by incubation with primary antibodies against Phospho-STAT5 (Tyr694) (C11C5) (Cell

Signaling Technology, #9359, dilution 1:500), STAT5 (D2O6Y) (Cell Signaling Technology, #94205, dilution 1:1000), Phospho-Jak1(Y1034/1035) (D7N4Z) (Cell Signaling Technology, #74129, dilution 1:500), Phospho-Jak3 (Y980/981) (D44E3) (Cell Signaling Technology, #5031, dilution 1:500) and Beta-actin (Cell Signaling Technology, #4970S, dilution 1:1000) for 1 hour at room temperature. After washing with TBST buffer three times, the membranes were incubated with horseradish-peroxidase–conjugated secondary antibody (Cell Signaling Technology, #7074S) for 40 min at room temperature. The membranes were washed with TBST buffer again six times and the immunoblot signal was detected with Pierce ECL Western blotting substrate (ThermoFisher Scientific) following the product's instruction. The intensity of immunoblot bands were quantified with ImageJ (*41*).

Statistical analysis

For experiments performed for bacterial two-hybrid (BACTH) assay, quantitative data were obtained from at least three biological replicates. For each biological replicate, up to ten technical replicates were performed for analysis. For experiments performed on BaF3 cells treated with different stimuli, at least two biological replicates and 1-2 technical replicates per biological replicate were performed for analysis. Statistical significance was calculated with GraphPad Prism 9.3.1 (Student's t-test; paired or unpaired test). Where relevant, statistical test results are indicated in the corresponding figures. ns: not significant, *$P \leq 0.05$, **$P \leq 0.01$, ***$P \leq 0.001$, ****$P \leq 0.0001$.

Transmembrane domain (TMD) sample preparation for NMR investigations

TMD expression, purification, and reconstitution in bicelles were performed following a previously published protocol (*45*).

Expression of fusion protein

The DNA sequences coding for the TMDs of mouse γc (residues 253-286), IL-7R (residues 236-266) and IL-9R (residues 268-298) and human IL-7R (residues 236-266) were synthesized by GenScript, codon optimized for *E. coli* expression. For the γc, amino acids M271 and C282 were mutated to valine and phenylalanine, respectively. For the human IL-7R, C261 was mutated to histidine based on sequence alignment across species for purification and better expression. The DNAs were cloned into the pMM-LR6 vector, fused at the C-terminus of the His_9-TrpLE tag

sequence with a methionine codon between the tag and the TMD sequence for tag cleavage. The TrpLE tag enables TMDs, which are very hydrophobic and potentially toxic to cells, to be driven into inclusion bodies, resulting in higher expression yields. BL21 DE3 (New England Biolabs) cells were transformed with the plasmids containing γcTMD or IL-7RTMD gene sequences following manufacturer's recommendations, whereas BL21 C43 cells were transformed with the IL-9RTMD containing plasmid and selected using 50 μg/ml of kanamycin. Precultures were grown in 100 ml of M9 minimal medium. Depending on the isotopic labeling required, M9 medium was composed of H_2O, 50 mM Na_2HPO_4, 25 mM KH_2PO_4, 10 mM NaCl, 2 mM $MgSO_4$, 0.1 mM $CaCl_2$, 4 mg/ml D-Glucose (Cambridge Isotope Laboratories, ref CLM-13965 for ^{13}C D-glucose), 1 mg/ml of ammonium chloride (Cambridge Isotope laboratories, ref NLM-467-5 for ^{15}N ammonium chloride), and 50 μg/ml of kanamycin sulphate. For perdeuterated samples (e.g., (^{15}N, ^{2}H)-labeled sample), the M9 medium was comprised of 99.8% D_2O (Cambridge Isotope Laboratories DLM-4-99.8-1000) and 4 mg/ml of deuterated glucose (D1,2,3,4,5,6,7 D-Glucose, ref DLM-20621) with all other components the same as above. Precultures were incubated at 37°C and 220 rpm, then used to inoculate 900 ml of the same medium and incubated further until the OD_{600} reached between 0.6 and 0.8. Protein expression was induced with 0.5 mM isopropyl β-D-thiogalatopyranoside (IPTG, Sigma-Aldrich) for IL-7RTMD and γcTMD or 1 mM IPTG for IL-9RTMD. IL-7RTMD and IL-9RTMD were expressed at 37°C overnight (∼18 hours) and γcTMD was expressed at 22°C overnight.

Purification of fusion protein

Cells were harvested by centrifuging 30 min at 8000*g* and 4°C, and resuspended in lysis buffer (50 mM Tris, pH 8.0, and 200 mM NaCl). Cells were then sonicated on ice for 10 min at 1-s intervals with 50% maximum amplitude. The resulting lysate was centrifuged for 30 min at 35,000*g* and 4°C. The pelleted inclusion bodies were resuspended in guanidine buffer (6 M guanidine–HCl, 50 mM Tris, pH 8.0, and 200 mM NaCl, filtered through a 0.22-mm MCE membrane, (MF-Millipore™) with 1% (vol/vol) Triton X-100 added) and dissolved using a glass tissue grinder until homogenous. The lysate was centrifuged one final time for 20 min at 35,000*g* and 4°C. The supernatant was then added to Ni-NTA resin (HisPur™Ni-NTA resin, Thermo Scientific) and thoroughly washed with dH_2O beforehand. The solution was left to incubate on a rotator gently for at least 2 hours or overnight. The mixture was transferred to a glass chromatography column

and purified by gravity flow. The flow through was discarded, and the resin was washed twice with 10 resin volumes of 8M urea, and then washed twice with 10 resin volumes of dH_2O. The target protein was eluted in four consecutive resin volumes of 90% formic acid.

Release of TMD by cyanogen bromide cleavage

Cyanogen bromide (CNBr) was used to cleave the His9-TrpLE tag from the TMD by hydrolyzing the peptide bond at the C-terminus of the methionine residue. Room temperature cyanogen bromide was added directly to the eluate (200 mg/ml), and vortexed until completely dissolved. The solution was left at room temperature, shielded from light, and under a gentle nitrogen stream for 1 hour. The reaction time here was carefully controlled to avoid formylation of the TMD. The mixture was then dialyzed twice against 100X volumes of water, for 40 min each time, in a 3.5-kDa dialysis cassette (Thermo Scientific). After dialysis, the solution was supplemented with dH_2O to aid freezing and lyophilized until completely dry (about 2 days).

TMD isolation by HPLC

Once fully lyophilized into a dry powder, the protein was dissolved with 4 ml of 90% formic acid and injected into a HPLC system. Purification was undertaken using a Zorbax 300SB-C3 column, 5 mm, 9.4×250 mm (Agilent), pre-equilibrated with a buffer of 5% isopropanol (Merck), 95% dH_2O, and 0.1% trifluoroacetic acid (Merck). Elution was performed with a gradient of 30 to 100% elution buffer (25% acetonitrile (Merck), 75% isopropanol, and 0.1% trifluoroacetic acid) in 140 ml at 2 ml/min. Elution peaks corresponding to the TMD of interest were collected and lyophilized. When making a mixed sample with two differently labeled TMDs, they were mixed at an approximative 1:1 molar ratio after elution from the Ni-NTA resin by formic acid and before cyanogen bromide cleavage. During the HPLC purification, the TMDs eluted as two separate peaks. The absorbance of the eluate was measured for each peak and they were mixed, again, at a 1:1 molar ratio after measurement of absorbance at 280 nm using a Nanodrop and prior to lyophilization.

Reconstitution of TMD in bicelles

Approximately 1–2 mg of dried TMD powder was resuspended in HFIP (1,1,1,3,3,3-Hexafluoro-2-propanol, Oakwood Chemical). Concurrently, 9 mg of DMPC (14:0 PC 1,2-dimyristoyl-sn-

glycero-3-phosphocholine, Avanti Polar Lipids) and 27 mg of DHPC (06:0 PC 1,2-dihexanoyl-sn-glycero-3-phosphocholine, Avanti Polar Lipids) were measured and dissolved in HFIP until homogenous. To obtain deuterated bicelles, d54-DMPC (Cortecnet, ref CD5012P025) and d22-DHPC (Cortecnet, ref CD5010P025) were used instead. If reconstituting the γcTMD and IL-9RTMD together, the amounts of lipid and detergent were doubled. The protein mixture was then added to the lipid–detergent mixture and the solution was dried under a gentle nitrogen stream for approximately 1 hour. The sample was then dried overnight by lyophilization to remove any remaining organic solvent. The dried film was resuspended in 3 ml of 8 M urea and dialyzed for a total of 6 hours against 1 liter of NMR buffer (50 mM phosphate buffer pH 6.7) in a 3.5-kDa dialysis cassette, changing the bath every 2 hours. DHPC was added regularly to the cassette to replace the detergent lost during dialysis (approximately 3–5 mg lost per hour). The protein was then concentrated in a 3-kDa centrifugal filter (Amicon Ultra 4, Ultracel 3K) at 8000*g* until a concentration of approximately 0.5 mM per TMD was reached. D_2O was added at 10% of final volume for frequency locking. The ratio (*q*) of DMPC to DHPC was verified by integrating the corresponding methyl peaks acquired by 1D ^{1}H NMR spectrum and adjusted accordingly for the q = 0.4-0.5. At this ratio, the diameter of the planar region of the bicelle was 40–45 Å.

Assignment of NMR Resonances

NMR data was collected at 303K on Bruker spectrometers operating at ^{1}H frequency of 900, 800, 700, or 600 MHz equipped with cryogenic probes. NMR data sets were processed using nmrPipe (*46*). NMR spectra were analyzed using XEASY (*47*) and CcpNmr Analysis v.2 (*48*). For sequence-specific assignment of backbone $^{1}H^{N}$, ^{15}N, $^{13}C^{\alpha}$, and $^{13}C'$ resonances of the three TMDs in this study, (^{15}N, ^{13}C, 85% ^{2}H)-labeled γcTMD, IL-7RTMD, and IL-9RTMD were purified and reconstituted in bicelles separately. Each of the three samples were used to record 3D TROSY-based HNCA, HN(CO)CA, HN(CA)CO and HNCO spectra (*49*, *50*) at ^{1}H frequency of 600 MHz. Complete assignment of the structured region was achieved for all three TMDs. Similarly, (^{15}N, ^{13}C)-labeled γcTMD, IL-7RTMD, and IL-9RTMD were purified and reconstituted in deuterated bicelles separately for the assignment of aliphatic and aromatic resonances of protein sidechains. Each of the three samples were used to record a 3D ^{15}N-edited NOESY-TROSY-HSQC (τNOE = 60 ms) and a 3D ^{13}C-edited NOESY-HSQC (τ_{NOE} = 100 ms) spectra at ^{1}H frequency of 700 MHz. The aliphatic proton resonances were assigned by comparing NOE patterns (specific to helix

structure) in ^{15}N-edited and ^{13}C-edited NOE strips. Finally, both backbone and sidechain assignments of γcTMD, IL-7RTMD, or IL-9RTMD alone were traced when mixed with its binding partner, which were further confirmed by NOE analysis of the heterodimeric complexes (see below).

Assignment of NOE Restraints

Due to the complexity associated with heterodimerization, assignment of intermolecular NOEs was challenging as it required preparation of multiple samples with different isotope labeling schemes in deuterated bicelles. For NOE analysis of γcTMD in complex with IL-7RTMD, we prepared samples of (^{15}N, ^{2}H)-labeled γcTMD mixed with (^{13}C)-labeled IL-7RTMD at 1:1 ratio and (^{15}N, ^{2}H)-labeled IL-7RTMD mixed with (^{13}C)-labeled γcTMD (fig. S6) for detecting complementary interchain NOEs. We first confirmed TMD heterodimerization in bicelles by performing a 2D NOE difference experiment at 700 MHz, which involved recording two interleaved ^{1}H-^{15}N TROSY-HSQC spectra: one preceded by 200 ms of NOE mixing at spin equilibrium (magnetization of amide and aliphatic protons in the same direction; spectrum A), and the other preceded by 200 ms of NOE mixing with the magnetization of ^{13}C-attached aliphatic protons selectively inverted by 8 ms of $^{1}J_{CH}$ modulation (spectrum B). Interchain NOEs between ^{15}N-attached protons of one chain and the ^{13}C-attached methyl protons of the opposing chain were revealed by subtracting spectrum A from B (Fig. 3A). Upon confirmation of specific heterotypic interaction, we then performed 3D ^{15}N-edited NOESY-TROSY (τ_{NOE} = 200 ms) and 3D ^{13}C-edited NOESY-HSQC (τ_{NOE} = 200 ms) at ^{1}H frequency of 900 MHz for each of the two samples above to assign the interchain NOE peaks. These complementary and reciprocal interchain NOEs identified the helix–helix packing interface. In addition to interchain NOEs between amide and methyl protons, we recorded another set of 3D ^{15}N-edited NOESY-TROSY (τ_{NOE} = 100 ms) and 3D ^{13}C-edited NOESY-HSQC (τ_{NOE} = 150 ms) at 900 MHz of a uniformly labeled sample with (^{15}N, ^{13}C)-labeled γcTMD mixed with (^{15}N, ^{13}C)-labeled IL-7RTMD at 1:1 ratio. This set of NOE data was used to assign local NOEs for the two TMDs as well as interchain NOEs between aliphatic protons (figs. S7 and S8).

For NOE analysis of γcTMD in complex with IL-9RTMD, we prepared samples of (^{15}N, ^{2}H)-labeled γcTMD mixed with (^{13}C)-labeled IL-9RTMD at 1:1 ratio and (^{15}N, ^{2}H)-labeled IL-9RTMD mixed with (^{13}C)-labeled γcTMD for detecting complementary interchain NOEs. Again, we first confirmed TMD heterodimerization in bicelles by performing the 2D NOE difference experiment described above at 700 MHz. After confirming specific heterodimerization, we performed 3D ^{15}N-edited NOESY-TROSY (τ_{NOE} = 200 ms) and 3D ^{13}C-edited NOESY-HSQC (τ_{NOE} = 200 ms) at ^{1}H frequency of 800 MHz for each of the two samples above to assign the interchain NOE peaks. These complementary and reciprocal interchain NOEs identified the helix–helix packing interface for the γcTMD–IL-9RTMD interaction.

Structure Calculation

The structures were generated using the program XPLOR-NIH (*51*). First, the monomer structures of γcTMD, IL-7RTMD, and IL-9RTMD were generated using the backbone dihedral restraints derived from ^{15}N, ^{1}H^{N}, ^{13}C$^{\alpha}$, and ^{13}C′ chemical shifts using the TALOS+ program (*52*). Second, the monomer structures and interchain NOEs between amide and methyl protons were used to generate crude structures of γcTMD–IL-7RTMD and γcTMD–IL-9RTMD heterodimers. Finally, the initial dimer structures were fed to the XPLOR-NIH for iterative refinement against all NMR restraints, while assigning more self-consistent inter- and intrachain NOEs in both ^{13}C-edited NOESY-HSQC and isotopically mixed NOE spectra after each iteration. This iterative process resulted in approximately five NOE restraints per residue for the structured regions of the two heterodimer complexes (table S1).

The XPLOR refinement used a simulated annealing (SA) protocol in which the temperature in the bath was cooled from 1000 to 200 K with steps of 20 K. The NOE restraints were enforced by flat-well harmonic potentials, with the force constant ramped from 2–30 (kcal/mol)/Å^2 during annealing. Backbone dihedral angle restraints were taken from the 'GOOD' dihedral angles from TALOS+ (*52*), all with a flat-well (± the corresponding uncertainties from TALOS+) harmonic potential with force constant ramped from 5–1000 (kcal/mol)/rad^2. For each of the two heterodimers, a total of 100 structures were calculated and 15 lowest energy structures were selected as the final structural ensemble (figs. S5D and S6D and table S1). The final ensemble of structures that satisfy all NMR restraints converged to root mean square deviation (RMSD) of

0.645 Å (backbone) and 1.234 Å (heavy atoms) for the γcTMD–IL-7RTMD dimer and RMSD of 0.711 Å (backbone) and 1.281 Å (heavy atoms) for the γcTMD–IL-9RTMD dimer (table S1).

Structural analysis of self-association of IL-7R TMD

To obtain structural information on the mode of TMD self-association of IL-7R, we used a construct of human IL-7R TMD containing residues 236–266, designated hIL-7RTMD. The protein fragment was expressed, purified, and reconstituted in bicelles as described above for other TMDs. We prepared an isotopically mixed sample of hIL-7RTMD in deuterated bicelles containing 50% (^{15}N, ^{13}C, ^{2}H)-labeled and 50% unlabeled protein. The final sample consisted of 1 mM hIL-7RTMD, 80 mM d54-DMPC, 200 mM d22-DHPC, and 50 mM phosphate (pH 6.7). This sample was used to record 3D TROSY-based HNCA, HN(CO)CA, HNCO, and resolution-maximized HN-HN ^{15}N-edited NOESY spectra for achieving sequence-specific assignment of backbone $^{1}H^{N}$, ^{15}N, $^{13}C^{\alpha}$, and $^{13}C'$ resonances. In addition, the same mixed sample was used to record a 3D ^{13}C-filtered/^{15}N-edited NOESY–TROSY spectrum for exclusive detection of intermolecular NOEs between the ^{15}N-attached amide protons of the labeled chain and the methyl groups of the unlabeled chain. Intermolecular NOEs indicated two nonoverlapping homodimer interactions (fig. S14A). The strong intermolecular NOEs involve the helix face with L255, I258, and L259. The weak NOEs involve the face with V253, V257, and A260. A model of the IL-7RTMD homodimer was constructed based on the strong interaction interface by optimizing VDW surface complementarity, showing that L255 is at the core of the packing interface (fig. S14B).

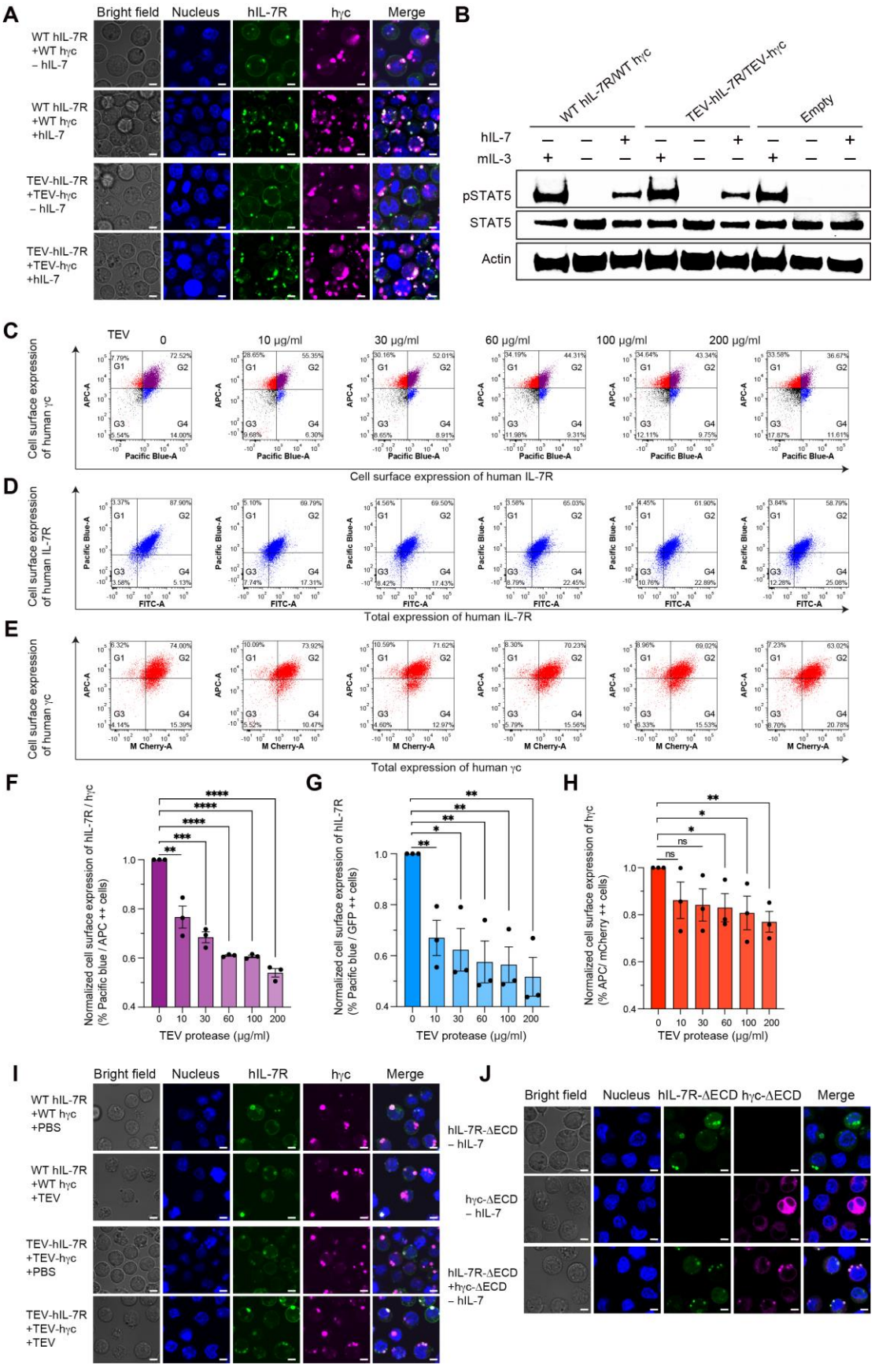
A
Bright field
Nucleus
hIL-7R
hγc
Merge
WT hIL-7R +WT hγc – hIL-7
WT hIL-7R +WT hγc +hIL-7
TEV-hIL-7R +TEV-hγc – hIL-7
TEV-hIL-7R +TEV-hγc +hIL-7
B
WT hIL-7R/WT hγc
TEV-hIL-7R/TEV-hγc
Empty
hIL-7
mIL-3
pSTAT5
STAT5
Actin
C
TEV
0
10 μg/ml
30 μg/ml
60 μg/ml
100 μg/ml
200 μg/ml
Cell surface expression of human γc
APC-A
Pacific Blue-A
Cell surface expression of human IL-7R
D
Cell surface expression of human IL-7R
FITC-A
Total expression of human IL-7R
E
Cell surface expression of human γc
M Cherry-A
Total expression of human γc
F
Normalized cell surface expression of hIL-7R / hγc (% Pacific blue / APC ++ cells)
TEV protease (μg/ml)
G
Normalized cell surface expression of hIL-7R (% Pacific blue / GFP ++ cells)
TEV protease (μg/ml)
H
Normalized cell surface expression of hγc (% APC/ mCherry ++ cells)
TEV protease (μg/ml)
I
Bright field
Nucleus
hIL-7R
hγc
Merge
WT hIL-7R +WT hγc +PBS
WT hIL-7R +WT hγc +TEV
TEV-hIL-7R +TEV-hγc +PBS
TEV-hIL-7R +TEV-hγc +TEV
J
Bright field
Nucleus
hIL-7R-ΔECD
hγc-ΔECD
Merge
hIL-7R-ΔECD – hIL-7
hγc-ΔECD – hIL-7
hIL-7R-ΔECD +hγc-ΔECD – hIL-7

fig. S1. Additional data on human IL-7R and γc activation by ectodomain removal

(**A**) Confocal images of BaF3 cells expressing WT receptors (WT hIL-7R-EGFP / WT hγc-mCherry) or TEV-site-inserted receptors (TEV-hIL-7R-EGFP / TEV-hγc-mCherry) without and with 50 ng/ml of hIL-7. hIL-7R are shown as green, and hγc are shown as magenta. The nuclei of 1×10^6 cells were stained with DAPI (blue). Three independent experiments were performed with two replicates per experiment. The images represent one of the two biological replicates with similar results. Scale bar: 5 μm. (**B**) hIL-7R signaling pathway activation detected by STAT5 phosphorylation in untransfected (Empty) BaF3 cells or BaF3 cells expressing WT receptors (WT hIL-7R / WT hγc) or TEV-site-inserted receptors (TEV-hIL-7R / TEV-hγc) after treatment with 50 ng/ml of hIL-7 or mIL-3. **(C)** Representative flow cytometry data of cell surface expression of both human IL-7R and γc after TEV treatment. BaF3 cells coexpressing TEV-hIL-7R-EGFP and TEV-hγc-mCherry were collected after treatment with different concentrations of TEV. Cell surface expression of TEV-hIL-7R-EGFP and TEV-hγc-mCherry was compared with Pacific blue-conjugated anti-hIL-7R antibody (A019D5, BioLegend #351306) and APC-conjugated anti-hγc antibody (TUGh4, BioLegend #338608) staining, respectively. Gate 1 (G1) represents APC+ cells; Gate 2 (G2) represents Pacific blue/APC ++ cells; Gate 3 (G3) represents negative cells; Gate 4 (G4) represents Pacific blue+ cells. Cell population percentage is labeled in each gate. **(D)** Surface expression of human IL-7R after TEV treatment in the same samples shown in (C). Gate 1 (G1) represents Pacific blue + cells; Gate 2 (G2) represents Pacific blue/EGFP ++ cells; Gate 3 (G3) represents negative cells; Gate 4 (G4) represents EGFP + cells. Cell population percentage is labeled in each gate. **(E)** Surface expression of human γc after TEV treatment in the same samples shown in (C). Gate 1 (G1) represents APC + cells; Gate 2 (G2) represents APC/mCherry ++ cells; Gate 3 (G3) represents negative cells; Gate 4 (G4) represents mCherry + cells. Cell population percentage is labeled in each gate. (**F**) Removal of ECD of both human IL-7R and γc as shown with bar plot of the G2 population fraction in (C) at different TEV protease concentration. The data are means ± SEM from three independent experiments with one technical replicate per experiment. Statistical significance: Student's *t* test; ** $P\leq0.01$; *** $P\leq0.001$; **** $P\leq0.0001$. (**G**) Removal of ECD of human IL-7R as shown with bar plot of the G2 population fraction in (D) at different TEV protease concentration. The data are means ± SEM from three independent experiments with one technical replicate per experiment. Statistical significance: Student's *t* test;

*$P \leq 0.05$; **$P \leq 0.01$. (**H**) Removal of ECD of human γc as shown with bar plot of the G2 population fraction in (E) at different TEV protease concentration. The data points are means ± SEM from three independent experiments with one technical replicate per experiment. Statistical significance: Student's *t* test; ns, not significant; *$P \leq 0.05$; **$P \leq 0.01$. (**I**) Confocal images of BaF3 cells expressing WT receptors (WT hIL-7R-EGFP / WT hγc-mCherry) or TEV-site-inserted receptors (TEV-hIL-7R-EGFP /TEV-hγc-mCherry) without and with 50 μg/ml of TEV protease. hIL-7R and hγc were shown in green and magenta, respectively. The nuclei of 1×10^6 cells were stained with DAPI (blue). Three independent experiments were performed with two replicates per experiment. The images represent one of two biological replicates with similar results. Scale bar: 5 μm. (**J**) Confocal images of BaF3 cells expressing ECD-deleted hIL-7R (hIL-7R-ΔECD-EGFP) or ECD-deleted hγc (hγc-ΔECD-mCherry) or coexpressing hIL-7R-ΔECD-EGFP with hγc-ΔECD-mCherry in the absence of cytokine. hIL-7R-ΔECD and hγc-ΔECD were shown in green and magenta, respectively. The nuclei of 1×10^6 cells were stained with DAPI (blue). Three independent experiments were performed with two replicates per experiment. The images represent one of two biological replicates with similar results. Scale bar: 5 μm.

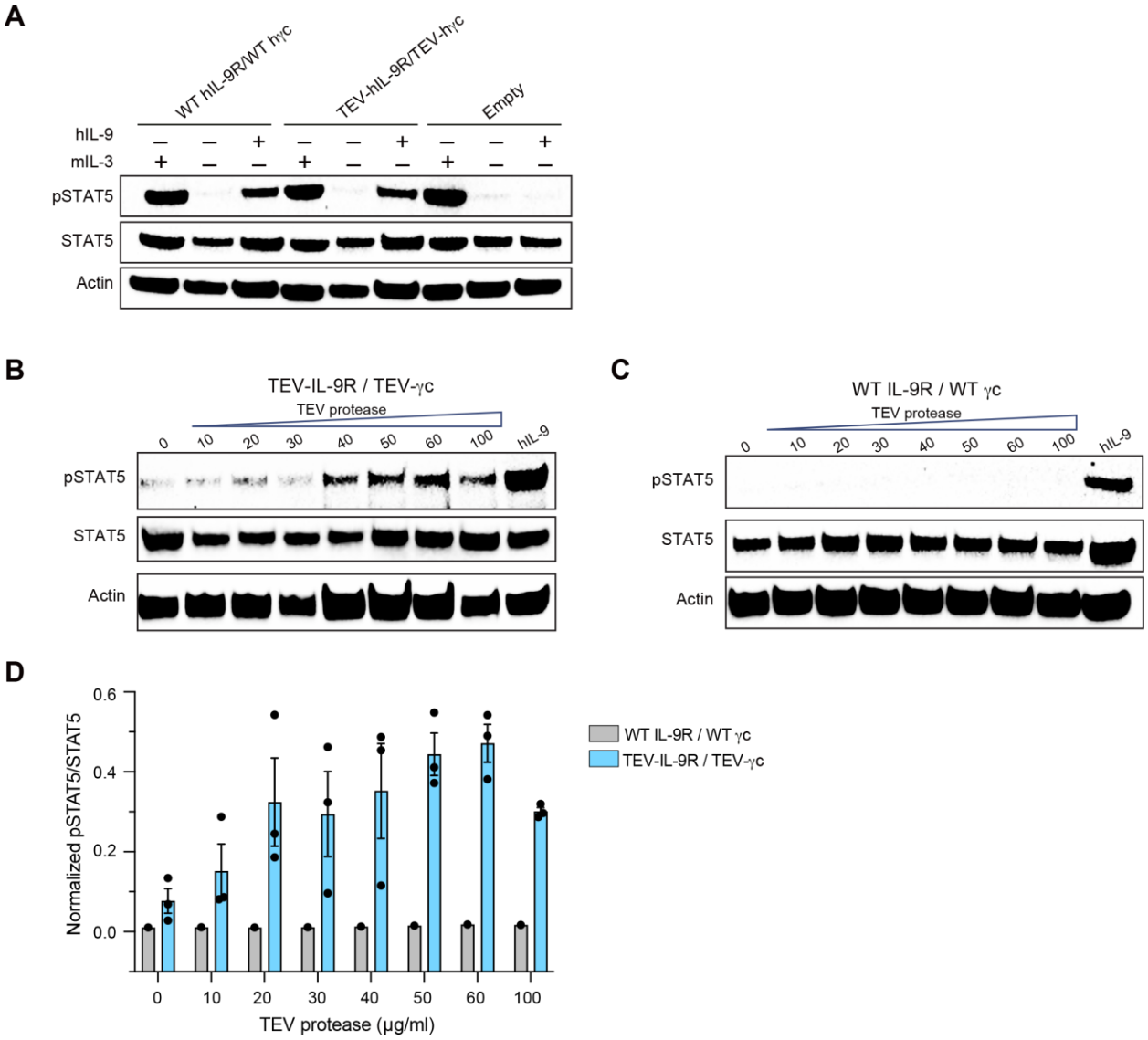

Fig. S2. Human IL-9R and γc activation by proteolytic removal of the ectodomains.

(**A**) IL-9R signaling pathway activation detected by STAT5 phosphorylation in untransfected (Empty) BaF3 cells or BaF3 cells expressing WT receptors (WT IL-9R / WT γc) or TEV-site-inserted receptors (TEV-IL-9R / TEV-γc) after treatment with 50 ng/ml of hIL-9 or mIL-3. **(B)** IL-9R pathway activation detected by immunoblotting of STAT5 phosphorylation (pSTAT5) in BaF3 cells coexpressing cleavable receptors (TEV-IL-9R / TEV-γc) after treatment with 0-100 μg/ml of TEV protease or 30 ng/ml of hIL-9. **(C)** IL-9R pathway activation detected by immunoblotting of STAT5 phosphorylation (pSTAT5) in BaF3 cells co-expressing uncleavable wild type receptors (WT IL-9R / WT γc) after treatment with 0-100 μg/ml of TEV protease or 30 ng/ml of hIL-9.

(D) Quantification of protease-induced pSTAT5 signals in (E) and (F) by ImageJ as pSTAT5/STAT5 intensity ratios, which are further normalized relative to that induced by IL-9. Results for TEV cleavable receptors (TEV-IL-9R / TEV-γc) are from three independent experiments and expressed as mean ± SEM and results for TEV uncleavable receptors (WT IL-9R / WT γc) are from one representative experiment.

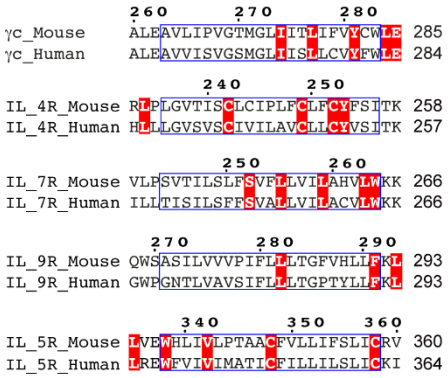
γc_Mouse ALEAVLIPVGTMGLIITLIFVYCWLE 285
γc_Human ALEAVVISVGSMGLIISLLCVYFWLE 284
IL_4R_Mouse RLPLGVTISCLCIPLFCLFCYFSITK 258
IL_4R_Human HLLLGVSVSCIVILAVCLLCYVSITK 257
IL_7R_Mouse VLPSVTILSLFSVFLLVILAHVLWKK 266
IL_7R_Human ILLTISILSFFSVALLVILACVLWKK 266
IL_9R_Mouse QWSASILVVVPIFLLLTGFVHLLFKL 293
IL_9R_Human GWPGNTLVAVSIFLLLTGPTYLLFKL 293
IL_5R_Mouse LVEWHLIVLPTAACFVLLIFSLICRV 360
IL_5R_Human LREWFVIVIMATICFILLILSLICKI 364

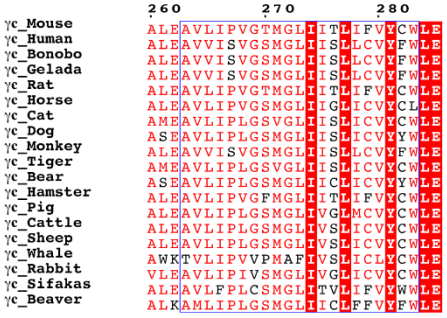
γc_Mouse ALEAVLIPVGTMGLIITLIFVYCWLE
γc_Human ALEAVVISVGSMGLIISLLCVYFWLE
γc_Bonobo ALEAVVISVGSMGLIISLLCVYFWLE
γc_Gelada ALEAVVISVGSMGLIISLLCVYFWLE
γc_Rat ALEAVLIPVGTMGLIITLIFVYCWLE
γc_Horse ALEAVLIPVGSMGLIIGLICVYCLLE
γc_Cat AMEAVLIPLGSVGLIISLICVYCWLE
γc_Dog ASEAVLIPLGSMGLIISLICVYYWLE
γc_Monkey ALEAVVISVGSMGLIISLLCVYFWLE
γc_Tiger AMEAVLIPLGSVGLIISLICVYCWLE
γc_Bear ASEAVLIPLGSMGLIICLICVYYWLE
γc_Hamster ALEAVLIPVGFMGLIITLIFVYCWLE
γc_Pig ALEAVLIPLGSMGLIVGLMCVYCWLE
γc_Cattle ALEAVLIPLGSMGLIVSLICVYCWLE
γc_Sheep ALEAVLIPLGSMGLIVSLICVYCWLE
γc_Whale AWKTVLIPVVPMAFIVSLICLYCWLE
γc_Rabbit VLEAVLIPIVSMGLIVGLICVYCWLE
γc_Sifakas ALEAVLFPLCSMGLITVLIFVYWWLE
γc_Beaver ALKAMLIPLGSMGLIICLFFVYFWLE

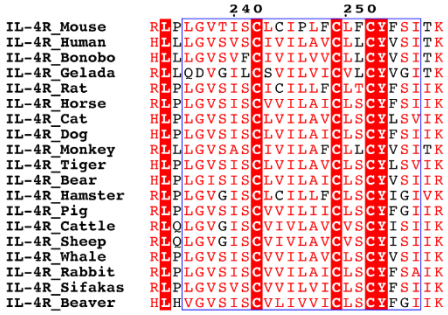
IL-4R_Mouse RLPLGVTISCLCIPLFCLFCYFSITK
IL-4R_Human HLLLGVSVSCIVILAVCLLCYVSITK
IL-4R_Bonobo HLLLGVSVFCIVILVVCLLCYVSITK
IL-4R_Gelada RLLQDVGILCSVILVICVLCYVGITK
IL-4R_Rat RLPLGVSISCICILLFCLTCYFSIIK
IL-4R_Horse RLPLGVSISCVVILAICLSCYFSIIK
IL-4R_Cat HLPLGVSISCLVILAVCLSCYLSVIK
IL-4R_Dog HLPLGVSISCLVILAICLSCYFSIIK
IL-4R_Monkey RLLLGVSASCIVILAFCLLCYVSITK
IL-4R_Tiger HLPLGVSISCLVILAVCLSCYLSVIK
IL-4R_Bear HLPLGISISCLVILAICLSCYVSIIR
IL-4R_Hamster RLPLGVGISCLCILLFCLSCYIGIVK
IL-4R_Pig RLPLGVSISCVVILIICLSCYFGIIR
IL-4R_Cattle RLQLGVGISCVIVLAVCVSCYISIIK
IL-4R_Sheep RLQLGVGISCVIVLAVCVSCYISIIK
IL-4R_Whale RLPLGVSISCVVILAVCLSCYVSIIK
IL-4R_Rabbit RLPLGVSISCVVILAICLSCYFSAIK
IL-4R_Sifakas RLPLGVSVSCVVILVICLSCYFSIIK
IL-4R_Beaver HLHVGVSISCVLIVVICLSCYFGIIK

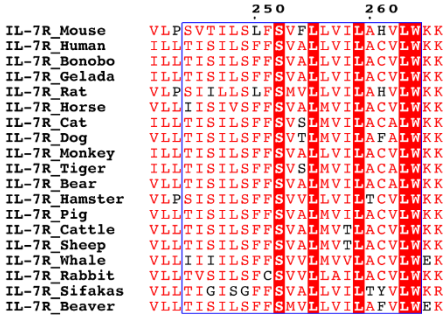
IL-7R_Mouse VLPSVTILSLFSVFLLVILAHVLWKK
IL-7R_Human ILLTISILSFFSVALLVILACVLWKK
IL-7R_Bonobo ILLTISILSFFSVALLVILACVLWKK
IL-7R_Gelada ILLTISILSFFSVALLVILACVLWKK
IL-7R_Rat VLPSIILLSLFSMVLLVILAHVLWKK
IL-7R_Horse VLLIISIVSFFSVALMVILACVLWKK
IL-7R_Cat ILLTISILSFFSVSLMVILACALWKK
IL-7R_Dog VLLTISILSFFSVTLMVILAFALWKK
IL-7R_Monkey ILLTISILSFFSVALLVILACVLWKK
IL-7R_Tiger ILLTISILSFFSVSLMVILACALWKK
IL-7R_Bear VLLTISILSFFSVALMVILACALWKK
IL-7R_Hamster VLPSISILSFFSVVLLVILTCVLWKK
IL-7R_Pig VLLTISILSFFSVALMVILACVLWKK
IL-7R_Cattle VLLTISILSFFSVALMVTLACVLWKK
IL-7R_Sheep VLLTISILSFFSVALMVTLACVLWKK
IL-7R_Whale VLLIIIILSFFSVVLMVVLACVLWEK
IL-7R_Rabbit VLLTVSILSFCSVVLLAILACVLWKK
IL-7R_Sifakas VLLTIGISGFFSVALLVILTYVLWKR
IL-7R_Beaver VLLTISILSFFSMVLLVILAFVLWEK

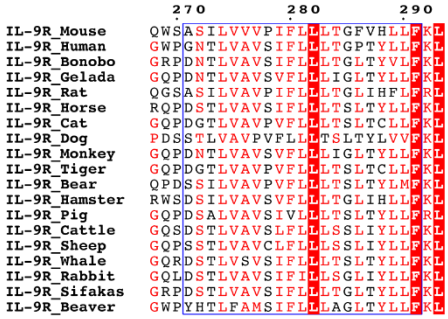
IL-9R_Mouse QWSASILVVVPIFLLLTGFVHLLFKL
IL-9R_Human GWPGNTLVAVSIFLLLTGPTYLLFKL
IL-9R_Bonobo GRPDNTLVAVSIFLLLTGLTYVLFKL
IL-9R_Gelada GQPDNTLVAVSVFLLLIGLTYLLFKL
IL-9R_Rat QGSASILVAVPIFLLLTGLIHFLFRL
IL-9R_Horse RQPDSTLVAVSIFLLLTSLTYLLFKL
IL-9R_Cat GQPDGTLVAVPVFLLLTSLTCLLFKL
IL-9R_Dog PDSSTLVAVPVFLLLTSLTYLVVFKL
IL-9R_Monkey GQPDNTLVAVSVFLLLIGLTYLLFKL
IL-9R_Tiger GQPDGTLVAVPVFLLLTSLTCLLFKL
IL-9R_Bear QPDSSILVAVPVFLLLTSLTYLMFKL
IL-9R_Hamster RWSDSILVAVSVFLLLTGLIHLLFKL
IL-9R_Pig GQPDSALVAVSIVLLLTSLTYLLFRL
IL-9R_Cattle GQSDSTLVAVSLFLLLSSLIYLLFKL
IL-9R_Sheep GQPSSTLVAVCLFLLLSSLIYLLFKL
IL-9R_Whale GQRDSTLVSVSIFLLLTSLTYLLFKL
IL-9R_Rabbit GQLDSTLVAVSIFILLSGLIYLLFKL
IL-9R_Sifakas GRPDSTLVAVSIFLLLTGLTYLLFKL
IL-9R_Beaver GWPYHTLFAMSIFLLLAGLTYLLFKL

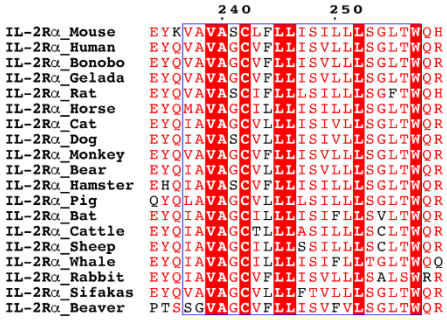
IL-2Rα_Mouse EYKVAVASCLFLLISILLLSGLTWQH
IL-2Rα_Human EYQVAVAGCVFLLISVLLLSGLTWQR
IL-2Rα_Bonobo EYQVAVAGCVFLLISVLLLSGLTWQR
IL-2Rα_Gelada EYQVAVAGCVFLLISVLLLSGLTWQR
IL-2Rα_Rat EYQVAVASCIFLLLSILLLSGFTWQH
IL-2Rα_Horse EYQMAVAGCILLLISILLLSGLTWQR
IL-2Rα_Cat EYQIAVAGCVLLLISIVLLSGLTWQR
IL-2Rα_Dog EYQIAVASCVLLLISIVLLSGLTWQR
IL-2Rα_Monkey EYQVAVAGCVFLLISVLLLSGLTWQR
IL-2Rα_Bear EYQIAVAGCVLLLISVLLLSGLTWQR
IL-2Rα_Hamster EHQIAVASCVFLLISILLLSGLTWQR
IL-2Rα_Pig QYQLAVAGCVLLLLSILLLSGLTWQR
IL-2Rα_Bat EYQIAVAGCILLLISIFLLSVLTWQR
IL-2Rα_Cattle EYQIAVAGCTLLLASILLLSCLTWQR
IL-2Rα_Sheep EYQIAVAGCILLLSSILLLSCLTWQR
IL-2Rα_Whale EYQIAVAGCILLLISIFLLTGLTWQQ
IL-2Rα_Rabbit EYQIAVAGCVFLLISVLLLSALSWRR
IL-2Rα_Sifakas EYQVAVAGCVLLLFTVLLLSGLTWQR
IL-2Rα_Beaver PTSSGVAGCVFLLISVFVLSGLTWQR

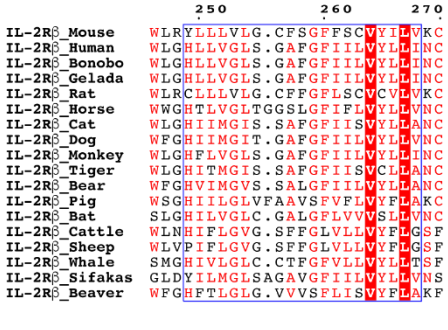
IL-2Rβ_Mouse WLRYLLLVLG.CFSGFFSCVYILVKC
IL-2Rβ_Human WLGHLLVGLS.GAFGFIILVYLLINC
IL-2Rβ_Bonobo WLGHLLVGLS.GAFGFIILVYLLINC
IL-2Rβ_Gelada WLGHLLVGLS.GAFGFIILVYLLINC
IL-2Rβ_Rat WLRCLLLVLG.CFFGFLSCVCVLVKC
IL-2Rβ_Horse WWGHTLVGLTGGSLGFIFLVYLLVNC
IL-2Rβ_Cat WLGHIIMGIS.SAFGFIISVYLLANC
IL-2Rβ_Dog WFGHIIMGIT.GAFGFIILVYLLVNC
IL-2Rβ_Monkey WLGHFLVGLS.GAFGFIILVYLLINC
IL-2Rβ_Tiger WLGHITMGIS.SAFGFIISVCLLANC
IL-2Rβ_Bear WFGHVIMGVS.SALGFIILVYLLANC
IL-2Rβ_Pig WSGHIILGLVFAAVSFVFLVYFLAKC
IL-2Rβ_Bat SLGHILVGLC.GALGFLVVVSLLVNC
IL-2Rβ_Cattle WLNHIFLGVG.SFFGLVLLVYFLGSF
IL-2Rβ_Sheep WLVPIFLGVG.SFFGLVLLVYFLGSF
IL-2Rβ_Whale SMGHIVLGLC.CTFGFVLLVYLLTSF
IL-2Rβ_Sifakas GLDYILMGLSAGAVGFIILVYLLVNS
IL-2Rβ_Beaver WFGHFTLGLG.VVVSFLISVYFLAKF

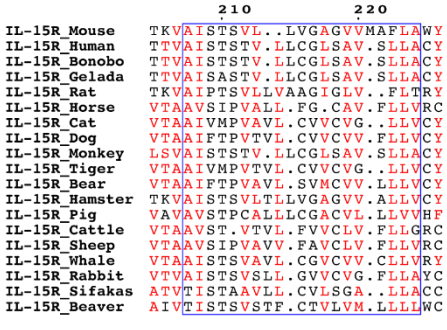
IL-15R_Mouse TKVAISTSVL..LVGAGVVMAFLAWY
IL-15R_Human TTVAISTSTV.LLCGLSAV.SLLACY
IL-15R_Bonobo TTVAISTSTV.LLCGLSAV.SLLACY
IL-15R_Gelada TTVAISASTV.LLCGLSAV.SLLACY
IL-15R_Rat TKVAIPTSVLLVAAGIGLV..FLTRY
IL-15R_Horse VTAAVSIPVALL.FG.CAV.FLLVRC
IL-15R_Cat VTAAIVMPVAVL.CVVCVG..LLVCY
IL-15R_Dog VTAAIFTPVTVL.CVVCVV.FLLVCY
IL-15R_Monkey LSVAISTSTV.LLCGLSAV.SLLACY
IL-15R_Tiger VTAAIVMPVTVL.CVVCVG..LLVCY
IL-15R_Bear VTAAIFTPVAVL.SVMCVV.LLLVCY
IL-15R_Hamster TKVAISTSVLTLLVGAGVV.ALLVCY
IL-15R_Pig VAVAVSTPCALLLCGACVL.LLVVHF
IL-15R_Cattle VTAAVST.VTVL.FVVCLV.FLLGRC
IL-15R_Sheep VTAAVSIPVAVV.FAVCLV.FLLVRC
IL-15R_Whale VTAAISTSVAVL.CGVCVV.CLLVRY
IL-15R_Rabbit VTVAISTSVSLL.GVVCVG.FLLAYC
IL-15R_Sifakas ATVTISTAAVLL.CVLSGA..LLACC
IL-15R_Beaver AIVTISTSVSTF.CTVLVM.LLLLWC

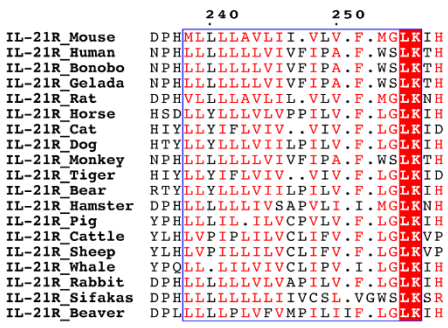
IL-21R_Mouse DPHMLLLAVLII.VLV.F.MGLKIH
IL-21R_Human NPHLLLLLLLVIVFIPA.F.WSLKTH
IL-21R_Bonobo NPHLLLLLLLVIVFIPA.F.WSLKTH
IL-21R_Gelada NPHLLLLLLLVIVFIPA.F.WSLKTH
IL-21R_Rat DPHVLLLLAVLIL.VLV.F.MGLKNH
IL-21R_Horse HSDLLYLLLVLVPPILV.F.LGLKIH
IL-21R_Cat HIYLLYIFLVIV..VIV.F.LGLKID
IL-21R_Dog HTYLLYLLLVIILPILV.F.LGLKIH
IL-21R_Monkey NPHLLLLLLLVIVFIPA.F.WSLKTH
IL-21R_Tiger HIYLLYIFLVIV..VIV.F.LGLKID
IL-21R_Bear RTYLLYLLLVIILPILV.F.LGLKIH
IL-21R_Hamster DPHLLLLLLIVSAPVLI.I.MGLKNH
IL-21R_Pig YPHLLLIL.ILVCPVLV.F.LGLKIH
IL-21R_Cattle YLHLVPIPLILVCLIFV.F.LGLKVP
IL-21R_Sheep YLHLVPILLILVCLIFV.F.LGLKVP
IL-21R_Whale YPQLL.LILVIVCLIPV.I.LGLKIH
IL-21R_Rabbit DPHLLLLLLVLVAPILV.F.LGLKIH
IL-21R_Sifakas DPHLLLLLLLLIIVCSL.VGWSLKSR
IL-21R_Beaver DPLLLLLPLVFVMPILIIF.LGLKIH

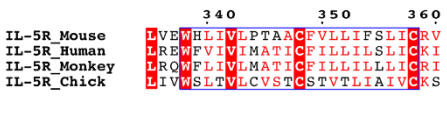
IL-5R_Mouse LVEWHLIVLPTAACFVLLIFSLICRV
IL-5R_Human LREWFVIVIMATICFILLILSLICKI
IL-5R_Monkey LRQWFLIVLMATICFILLILLLICRI
IL-5R_Chick LIVWSLTVLCVSTCSTVTLIAIVCKS

fig. S3. Sequence alignment of TMDs across species of the γc family receptors and IL-5R from the βc family

The TMD sequences of γc family receptors and the βc family member IL-5R are aligned using COBALT (*53*) and colored according to identity percentage. Residues with high similarity across species are shown in red. The 100% conserved residues are shown in white with red background. Transmembrane regions are highlighted with blue boxes.

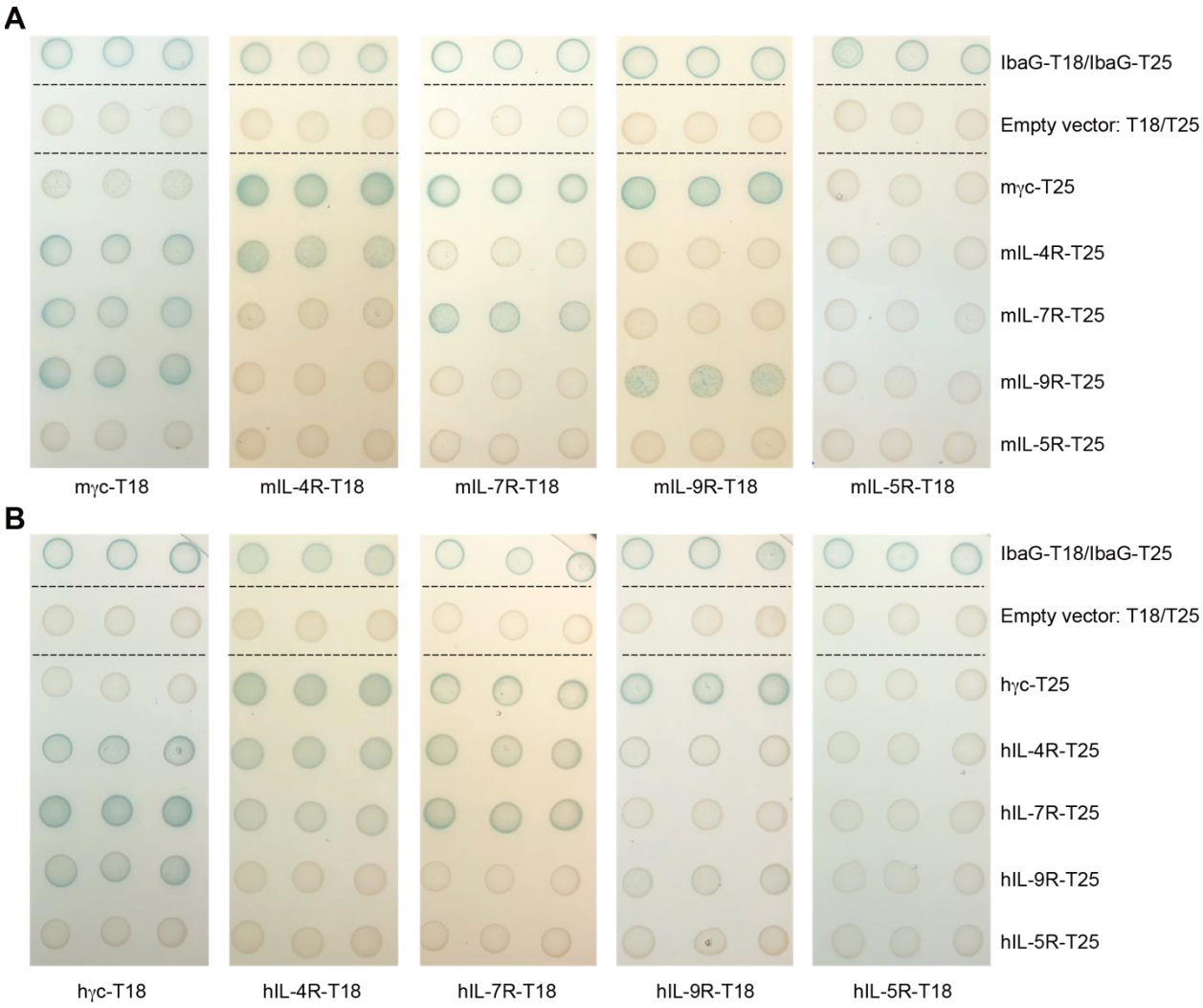

fig. S4. Additional BACTH analysis of TMD interactions for mouse and human IL-4R, IL-7R, IL-9R, and γc

(**A**) BACTH analysis of TMD interactions for representative γc family receptors including γc, IL-4R, IL-7R and IL-9R as well as the βc family receptor IL-5R. (**B**) Same as in (A) for TMD sequences from human. Three colonies were tested for each TMD-TMD combination. IbaG fused with T18 and T25 (IbaG-T18/IbaG-T25) was used as the positive control as previously published (*40*). Coexpression of empty vectors of T18 and T25 was used as the negative control. Blue colonies indicate TMD-TMD association in the bacteria's inner membrane.

A

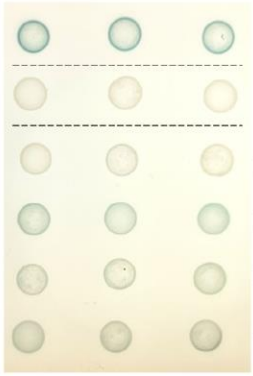

IbaG-T18/IbaG-T25

Empty vector: T18/T25

hγc-T18/hγc-T25

hIL-2Rα-T18/hIL-2Rα-T25

hIL-2Rα-T18/hγc-T25

hγc-T18/hIL-2Rα-T25

B

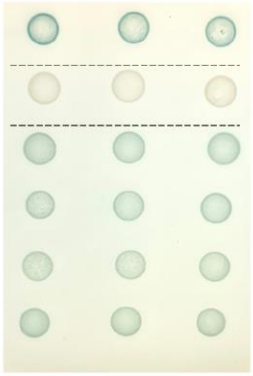

IbaG-T18/IbaG-T25

Empty vector: T18/T25

hIL-2Rα-T18/hIL-2Rα-T25

hIL-2Rβ-T18/hIL-2Rβ-T25

hIL-2Rα-T18/hIL-2Rβ-T25

hIL-2Rβ-T18/hIL-2Rα-T25

C

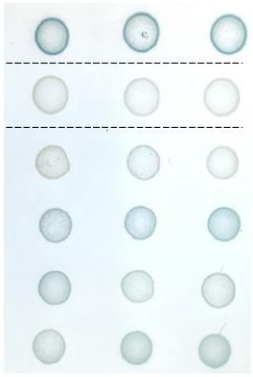

IbaG-T18/IbaG-T25

Empty vector: T18/T25

hγc-T18/hγc-T25

hIL-2Rβ-T18/hIL-2Rβ-T25

hIL-2Rβ-T18/hγc-T25

hγc-T18/hIL-2Rβ-T25

D

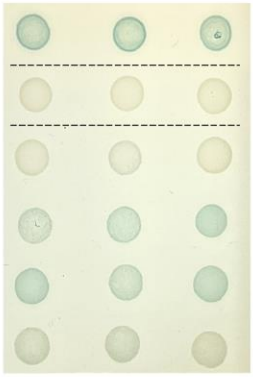

IbaG-T18/IbaG-T25

Empty vector: T18/T25

hIL-15R-T18/hIL-15R-T25

hIL-2Rβ-T18/hIL-2Rβ-T25

hIL-15R-T18/hIL-2Rβ-T25

hIL-2Rβ-T18/hIL-15R-T25

E

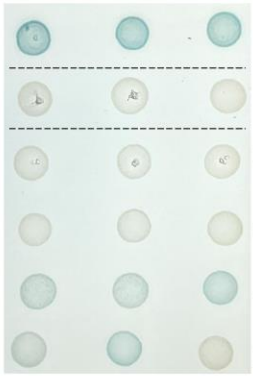

IbaG-T18/IbaG-T25

Empty vector: T18/T25

hγc-T18/hγc-T25

hIL-15R-T18/hIL-15R-T25

hIL-15R-T18/hγc-T25

hγc-T18/hIL-15R-T25

F

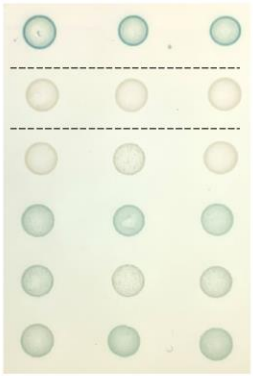

IbaG-T18/IbaG-T25

Empty vector: T18/T25

hγc-T18/hγc-T25

hIL-21R-T18/hIL-21R-T25

hIL-21R-T18/hγc-T25

hγc-T18/hIL-21R-T25

G

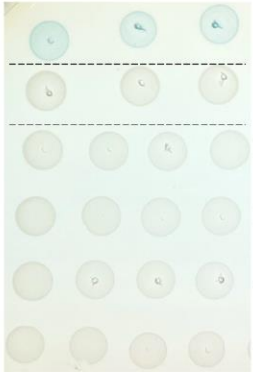

IbaG-T18/IbaG-T25

Empty vector: T18/T25

hβc-T18/hβc-T25

hIL-5R-T18/hIL-5R-T25

hIL-5R-T18/hβc-T25

hβc-T18/h-IL-5R-T25

fig. S5. Additional BACTH analysis of TMD interactions for human IL-2Rα, IL-2Rβ, IL-15R, IL-21R, and γc, as well as IL-5R and βc

(**A-G**) BACTH analysis of TMD interactions for γc family receptors including γc, IL-2Rα, IL-2Rβ, IL-15R and IL-21R as well as the βc family receptors βc and IL-5R from human. Three or four colonies were tested for each of the TMD-TMD combinations. IbaG fused with T18 and T25 (IbaG-T18/IbaG-T25) was used as the positive control as previously published (*40*). Coexpression of empty vectors of T18 and T25 was used as the negative control. Blue colonies indicate TMD-TMD association in the bacteria's inner membrane.

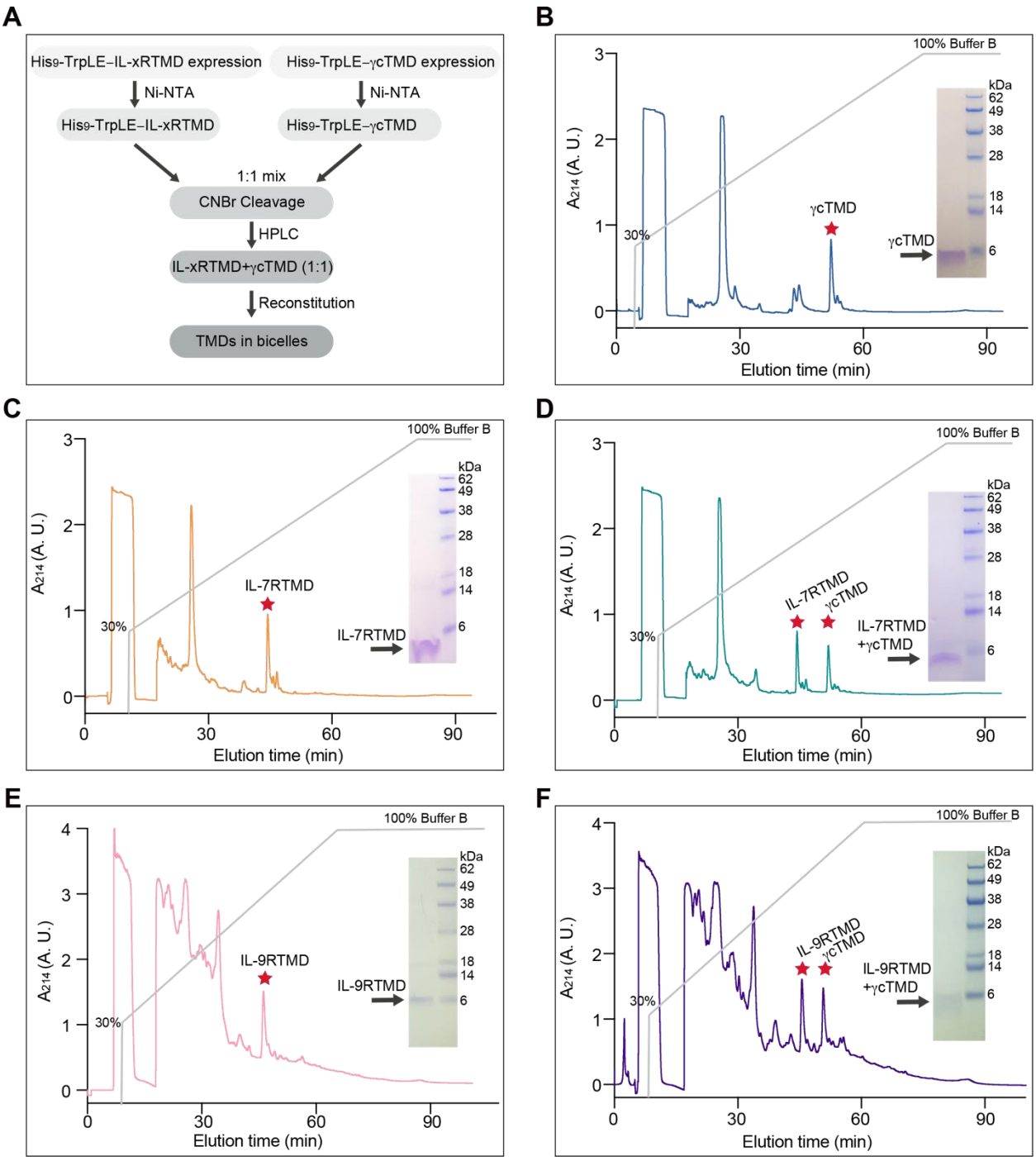

fig. S6. Purification of γcTMD, IL-7RTMD, IL9R-TMD and mixed TMDs

(**A**) Overview of the steps for mixed TMDs expression and purification (see Supplementary Materials and Methods for a detailed description). (**B**) Reverse-phase HPLC purification of γcTMD from CNBr-cleaved TrpLE-γcTMD fusion protein on Zorbax SB-C3 column with a

gradient from 95% dH2O, 5% isopropanol (IPA), 0.1% trifluoroacetic acid (TFA) (buffer A) to 75% IPA, 25% acetonitrile, 0.1% TFA (buffer B). (**C**) Same as in (B) for IL-7RTMD. (**D**) Same as in (B) for mixed IL-7RTMD with γcTMD. (**E**) Same as in (B) for IL-9RTMD. (**F**) Same as in (B) for mixed IL-9RTMD with γcTMD. The purity of the TMDs was verified by SDS-PAGE.

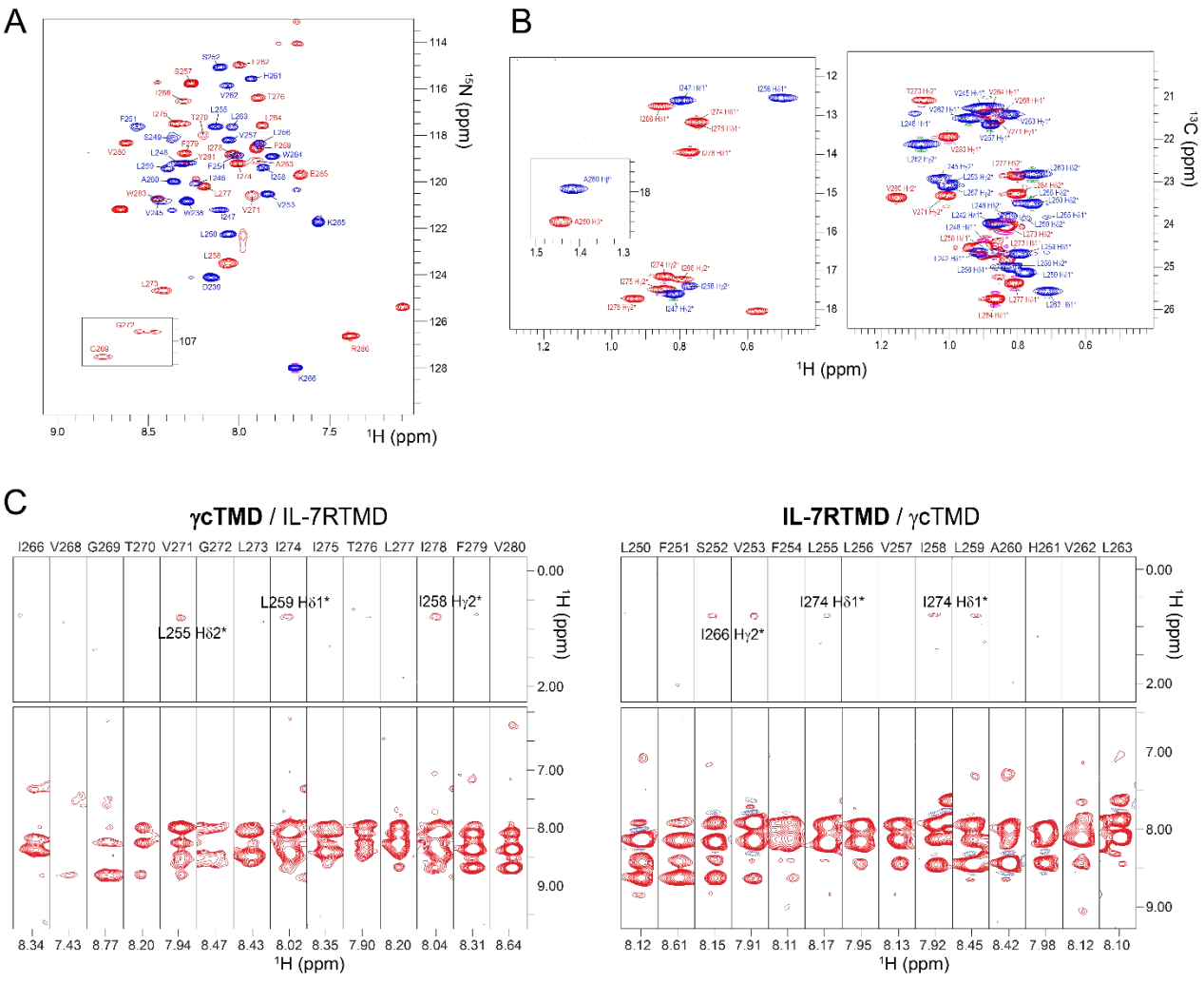

fig. S7. NMR characterization of the γcTMD / IL-7RTMD complex

(**A**) Overlay of ^{1}H-^{15}N TROSY-HSQC spectra of (^{15}N, ^{2}H) γcTMD in complex with ^{13}C IL-7RTMD (red) and the reciprocal sample of (^{15}N, ^{2}H) IL-7RTMD in complex with ^{13}C γcTMD (blue), recorded at 303K at ^{1}H frequency of 900 MHz. The glycine peaks are folded. (**B**) Overlay of ^{1}H-^{13}C HSQC spectra (methyl groups) of ^{13}C γcTMD in complex with (^{15}N, ^{2}H) IL-7RTMD (red) and ^{13}C IL-7RTMD in complex with (^{15}N, ^{2}H) γcTMD (blue). (**C**) Strips from 3D ^{15}N-edited NOESY–TROSY spectra of (^{15}N, ^{2}H) γcTMD / (^{13}C) IL-7RTMD (left) and (^{15}N, ^{2}H) IL-7RTMD / (^{13}C) γcTMD (right) showing interchain NOEs between the amide protons of ^{15}N-labeled and fully deuterated chain and the methyl protons of the ^{13}C-labeled chain. The spectra were recorded at 303 K at ^{1}H frequency of 900 MHz. (**D**) Ensemble of 15 lowest energy structures from 100 structures calculated using all NMR-derived restraints in table S1. Protons are not displayed for clarity. Residues included in the superposition are 262–284 of γcTMD and 245–265 of IL-7RTMD.

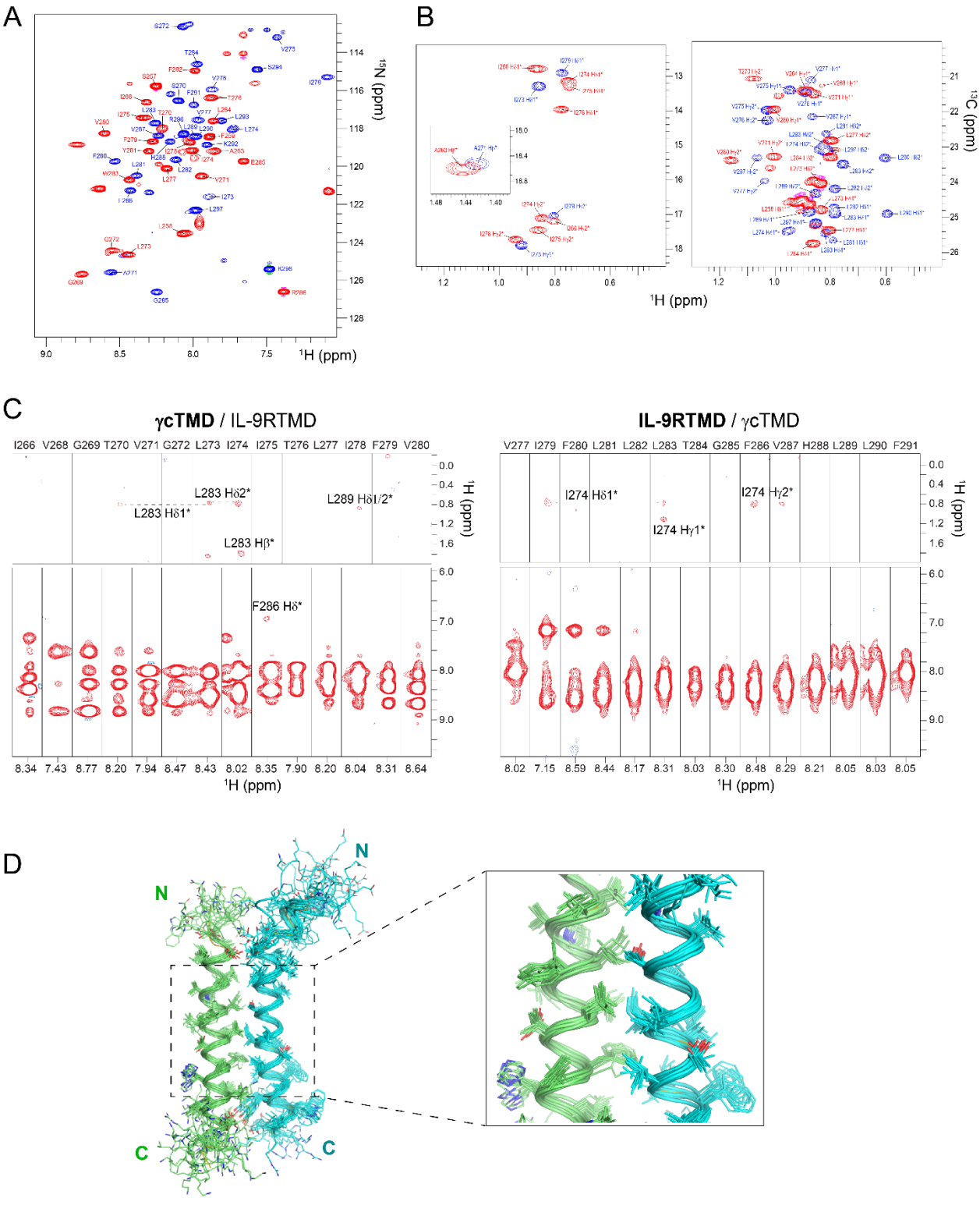

fig. S8. NMR characterization of the γcTMD / IL-9RTMD complex

(**A**) Overlay of ^{1}H-^{15}N TROSY-HSQC spectra of (^{15}N, ^{2}H) γcTMD in complex with ^{13}C IL-9RTMD (red) and the reciprocal sample of (^{15}N, ^{2}H) IL-9RTMD in complex with ^{13}C γcTMD (blue), recorded at 303K at ^{1}H frequency of 800 MHz. The glycine peaks are folded. (**B**) Overlay of ^{1}H-^{13}C HSQC spectra (methyl groups) of ^{13}C γcTMD in complex with (^{15}N, ^{2}H) IL-9RTMD (red) and ^{13}C IL-9RTMD in complex with (^{15}N, ^{2}H) γcTMD (blue). (**C**) Strips from 3D ^{15}N-edited NOESY-TROSY spectra of (^{15}N, ^{2}H) γcTMD / (^{13}C) IL-9RTMD (left) and (^{15}N, ^{2}H) IL-9RTMD / (^{13}C) γcTMD (right) showing interchain NOEs between the amide protons of ^{15}N labeled and fully deuterated chain and the methyl protons of the ^{13}C-labeled chain. The spectra were recorded at 303 K at ^{1}H frequency of 800 MHz. (**D**) Ensemble of 15 lowest energy structures from 100 structures calculated using all NMR-derived restraints in table S1. Protons are not displayed for clarity. Residues included in the superposition are 262–284 of γcTMD and 271–293 of IL-9RTMD.

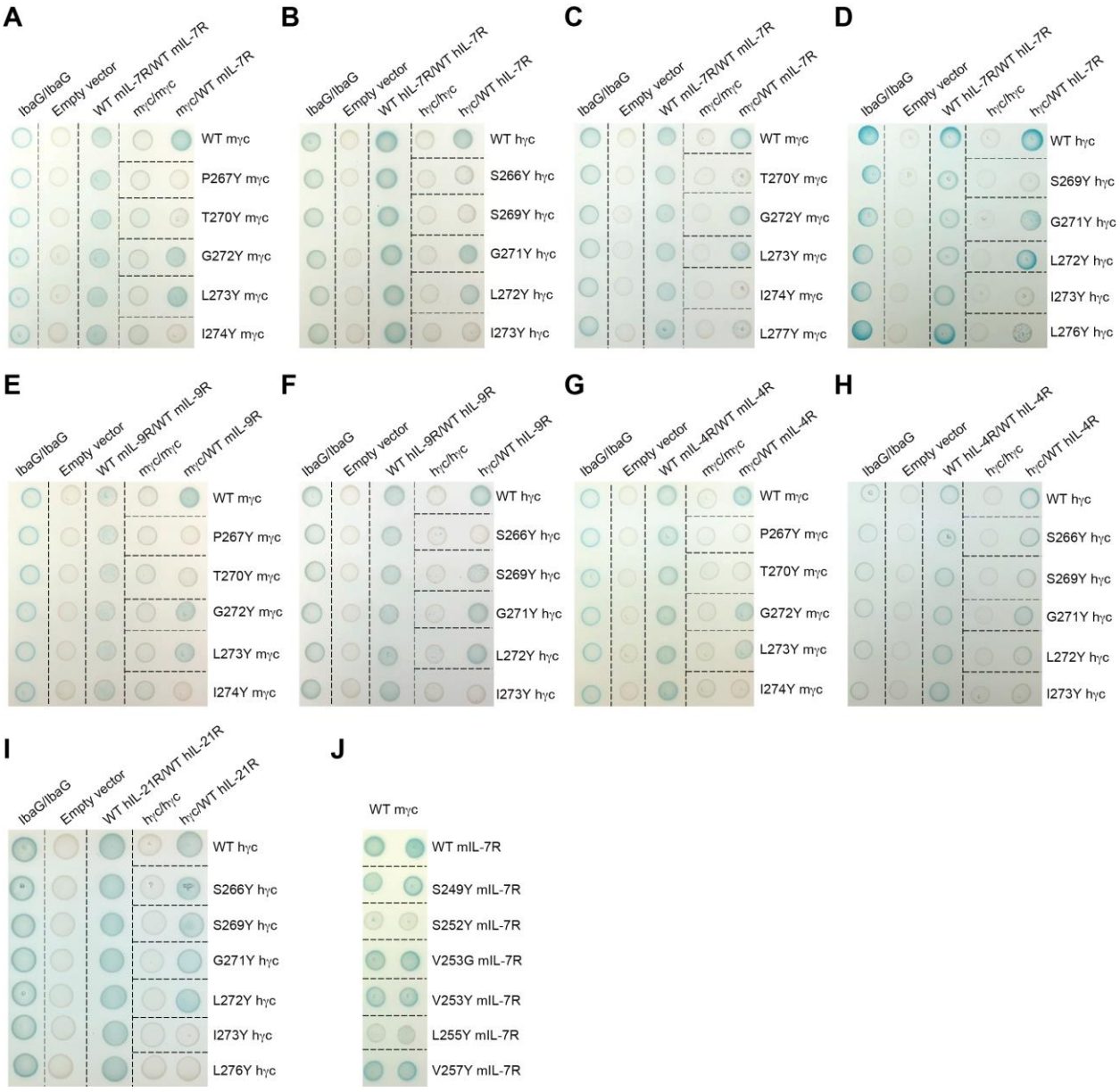

fig. S9. Additional results of site-directed mutagenesis and effect on TMD interaction

(**A** to **D**) Raw images of BACTH analysis of the effect of γcTMD mutations (P267Y, T270Y, G272Y, L273Y, I274Y, and L277Y in mouse γcTMD, and the corresponding mutations S266Y, S269Y, G271Y, L272Y, I273Y, and L276Y in human) on γcTMD association with mouse (A and C) and human (B and D) WT IL-7RTMD. (**E** and **F**) Same as in (A) and (B) for WT IL-9RTMD. (**G** and **H**) Same as in (A) and (B) for WT IL-4RTMD. (**I**) Same as in (B) and (D) for human WT IL-21RTMD. (**J**) Raw image of BACTH analysis of the effect of mouse IL-7RTMD mutations on

association with WT mouse γcTMD. IbaG fused with T18 and T25 (IbaG-T18/IbaG-T25) was used as the positive control as previously published (*40*). Coexpression of empty vectors of T18 and T25 was used as the negative control. Blue colonies indicate TMD–TMD association in the bacteria inner membrane.

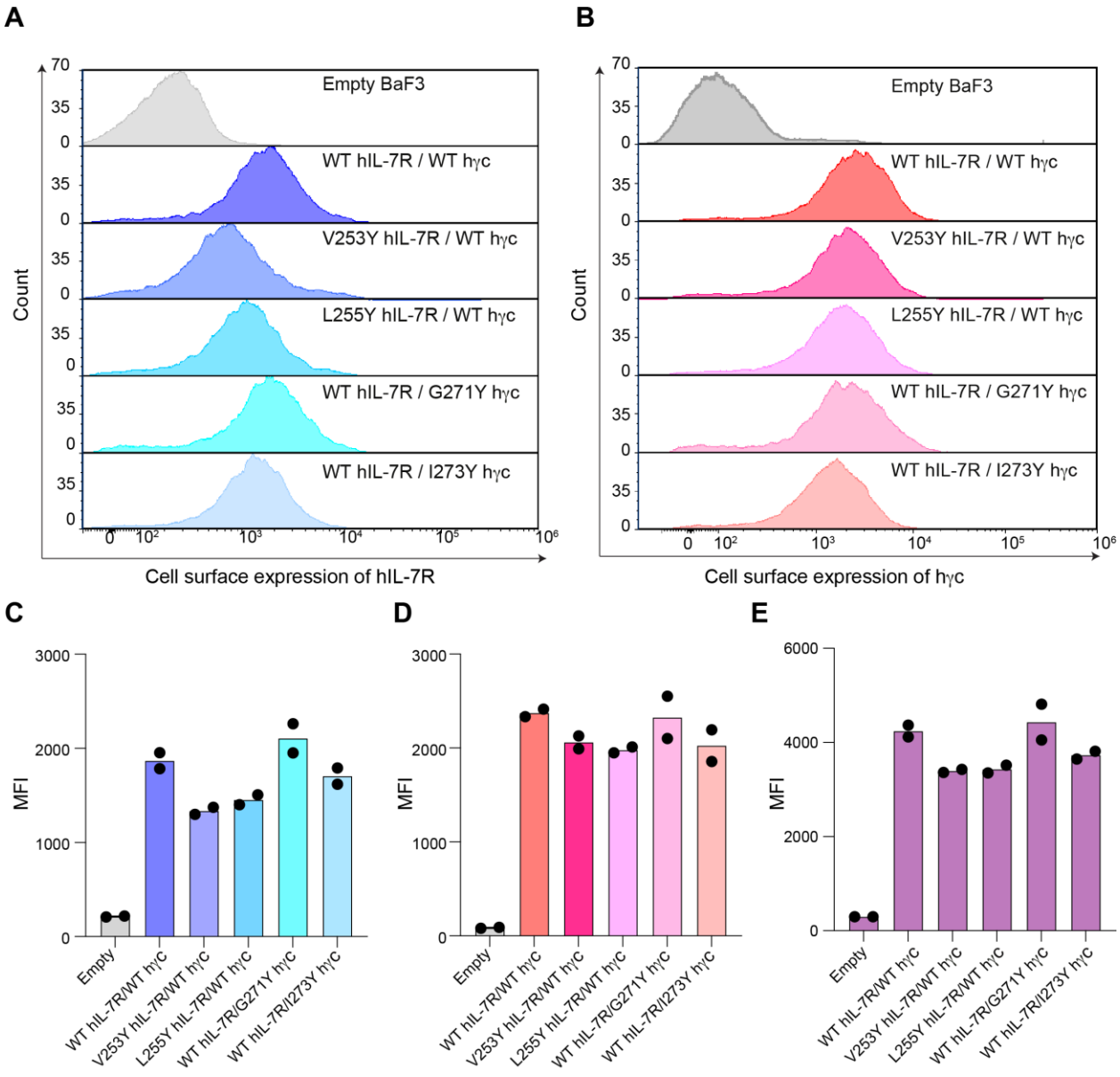

fig. S10. Flow cytometry analysis of cell surface coexpression of WT or mutants of IL-7R with WT or mutants of γc

(**A** and **B**) Quantification of cell surface expression level of hIL-7R variants and γc, respectively, by flow cytometry. Untransfected (Empty) BaF3 cells were used as negative controls. (**C**) Bar graphs showing geometric mean fluorescence intensity for IL-7R surface expression. The data are means from two independent experiments. (**D**) Bar graphs showing geometric mean fluorescence intensity for γc surface expression. The data are means from two independent experiments. (**E**)

Bar graphs showing geometric mean fluorescence intensity for coexpression of IL-7R and γc on the cell surface. The data are means from two independent experiments.

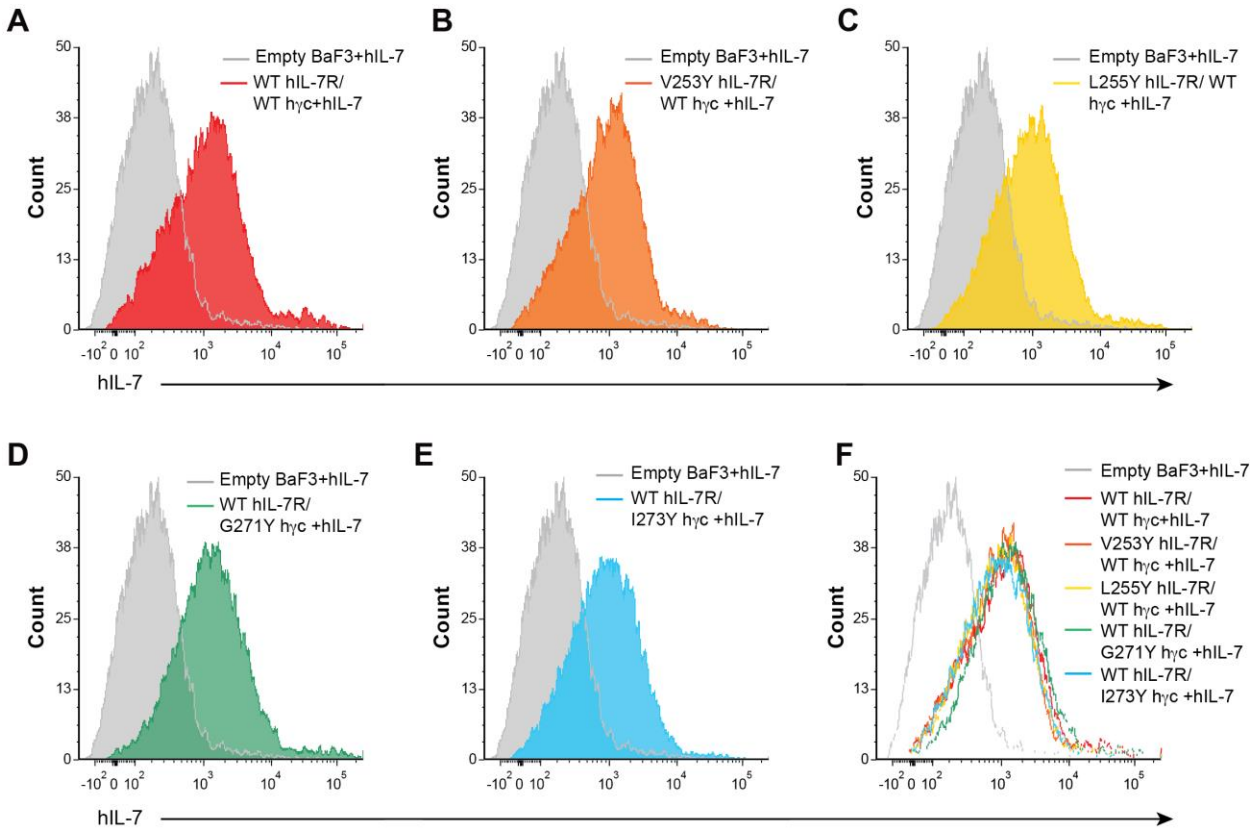

fig. S11. Flow cytometry analysis of hIL-7 binding to WT IL-7R and hγc and mutants

(**A**) Binding of hIL-7 to BaF3 cells coexpressing WT hIL-7R and WT hγc as analyzed by flow cytometry. Untransfected cells were used as a control. The experiment was repeated twice, and both showed very similar results. (**B**) Same as in (A) for V253Y hIL-7R coexpressed with WT hγc. (**C**) Same as in (A) for L255Y hIL-7R coexpressed with WT hγc. (**D**) Same as in (A) for WT hIL-7R coexpressed with G271Y hγc. (**E**) Same as in (A) for WT hIL-7R coexpressed with I273Y hγc. (**F**) Overlay comparison of hIL-7 binding for WT and all mutant receptors.

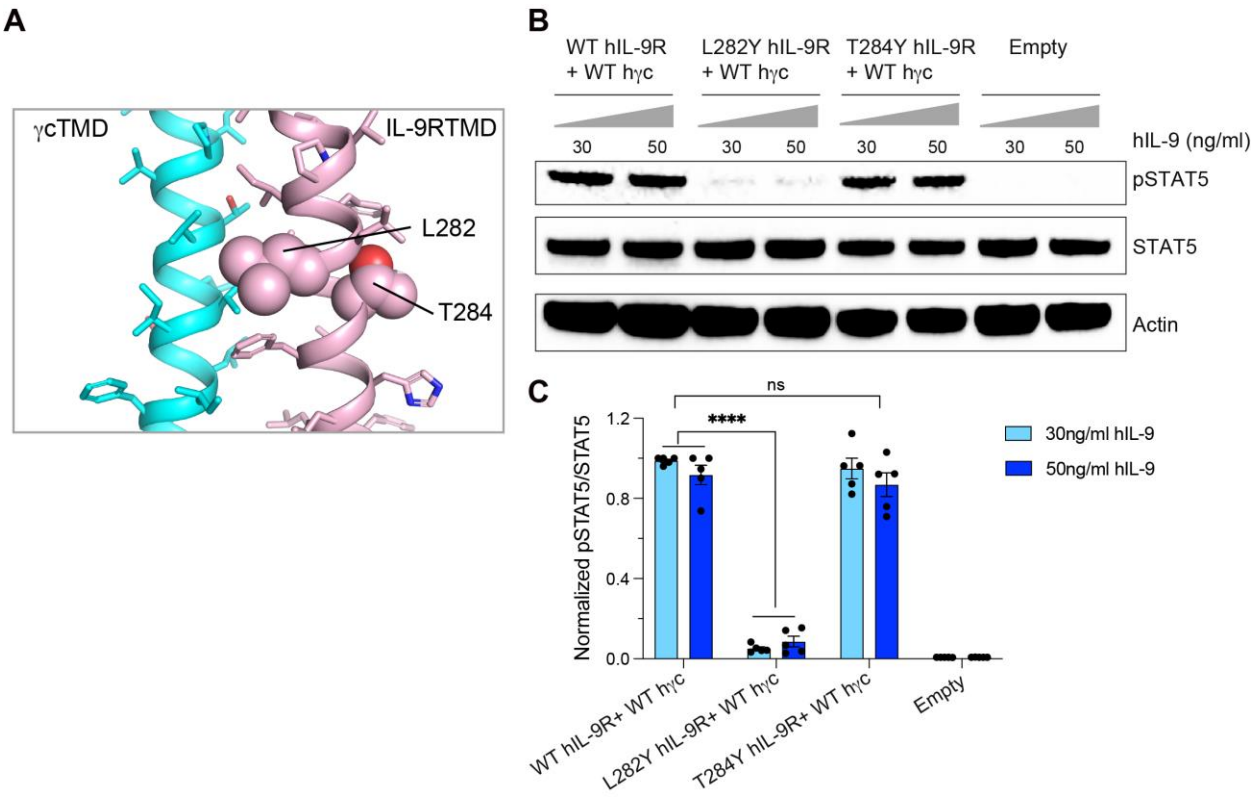

fig. S12. Specific TMD heterodimerization is required for ligand-induced IL-9R signaling

(**A**) Ribbon representation of the γcTMD / IL-9RTMD heterodimer structure showing the positions of the TMD residues of IL-9R (sphere) that were tested for ligand-induced receptor signaling. Specifically, L282 of IL-9R are important for the knob-into-hole mechanism whereas T284 of IL-9R are not involved in heterodimerization. (**B**) Phosphorylation of STAT5 in BaF3 cells coexpressing WT hγc with WT hIL-9R or hIL-9R mutants after 5 hours of cytokine deprivation and treatment with 30 or 50 ng/ml of hIL-9. Untransfected (empty) BaF3 cells were used as negative control. (**C**) Quantification of pSTAT5/STAT5 signal ratio in (B) by ImageJ, which are further normalized relative to that of WT hIL-9R / WT hγc receptors. Results are from five independent experiments and expressed as means ± SEM. Statistical significance: Student's *t* test; ns, not significant; ****$P \leq 0.0001$.

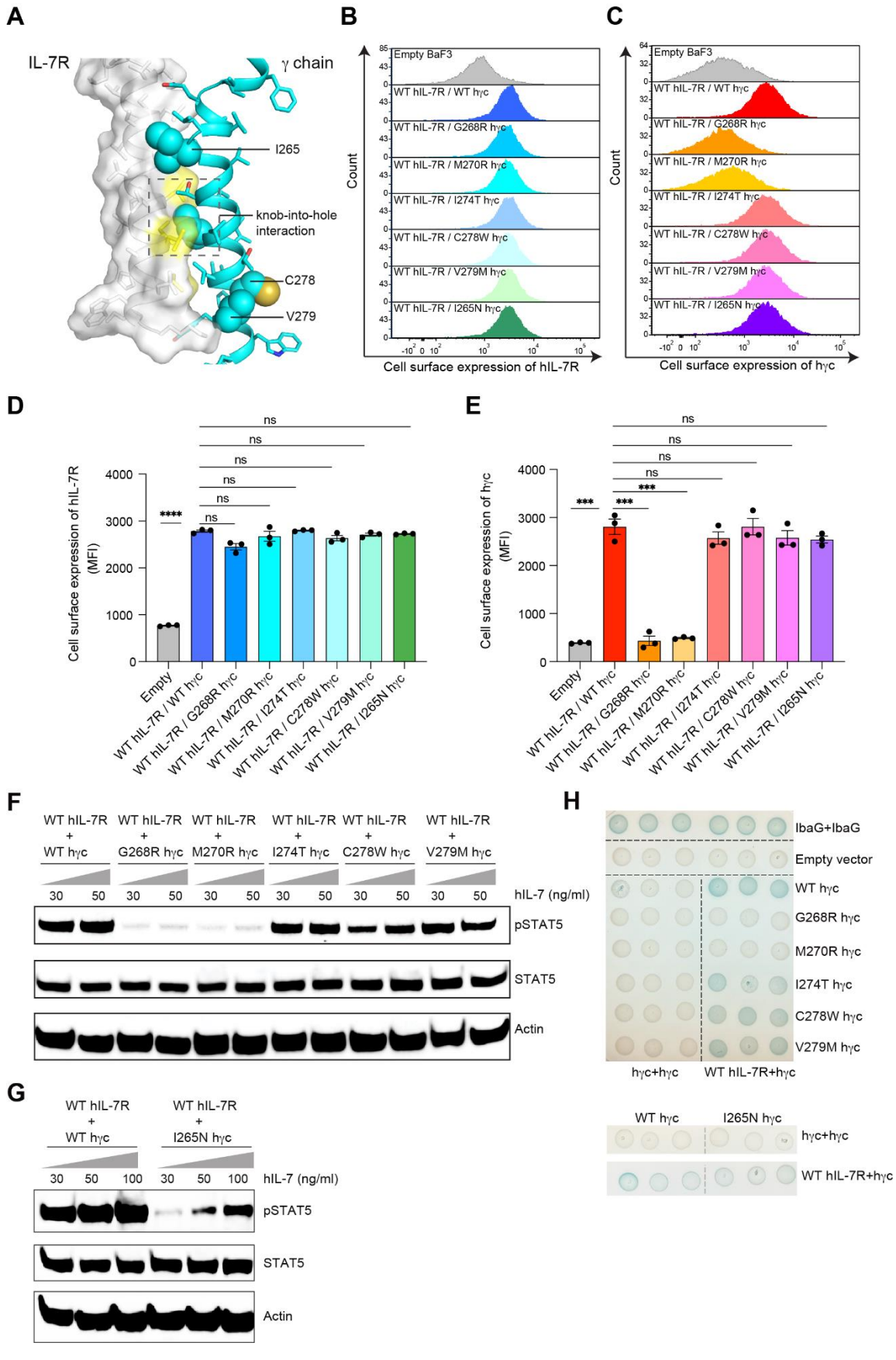
A
IL-7R
γ chain
I265
knob-into-hole interaction
C278
V279
B
Empty BaF3
WT hIL-7R / WT hγc
WT hIL-7R / G268R hγc
WT hIL-7R / M270R hγc
WT hIL-7R / I274T hγc
WT hIL-7R / C278W hγc
WT hIL-7R / V279M hγc
WT hIL-7R / I265N hγc
Count
Cell surface expression of hIL-7R
C
Empty BaF3
WT hIL-7R / WT hγc
WT hIL-7R / G268R hγc
WT hIL-7R / M270R hγc
WT hIL-7R / I274T hγc
WT hIL-7R / C278W hγc
WT hIL-7R / V279M hγc
WT hIL-7R / I265N hγc
Count
Cell surface expression of hγc
D
Cell surface expression of hIL-7R (MFI)
Empty
WT hIL-7R / WT hγc
WT hIL-7R / G268R hγc
WT hIL-7R / M270R hγc
WT hIL-7R / I274T hγc
WT hIL-7R / C278W hγc
WT hIL-7R / V279M hγc
WT hIL-7R / I265N hγc
E
Cell surface expression of hγc (MFI)
Empty
WT hIL-7R / WT hγc
WT hIL-7R / G268R hγc
WT hIL-7R / M270R hγc
WT hIL-7R / I274T hγc
WT hIL-7R / C278W hγc
WT hIL-7R / V279M hγc
WT hIL-7R / I265N hγc
F
WT hIL-7R + WT hγc
WT hIL-7R + G268R hγc
WT hIL-7R + M270R hγc
WT hIL-7R + I274T hγc
WT hIL-7R + C278W hγc
WT hIL-7R + V279M hγc
hIL-7 (ng/ml)
pSTAT5
STAT5
Actin
G
WT hIL-7R + WT hγc
WT hIL-7R + I265N hγc
hIL-7 (ng/ml)
pSTAT5
STAT5
Actin
H
IbaG+IbaG
Empty vector
WT hγc
G268R hγc
M270R hγc
I274T hγc
C278W hγc
V279M hγc
hγc+hγc
WT hIL-7R+hγc
WT hγc
I265N hγc
hγc+hγc
WT hIL-7R+hγc

fig. S13. Effect of naturally occurring hγc TMD mutations on hIL-7R signaling and on TMD heterodimerization between hγc and hIL-7R

(**A**) The heterodimer model of human γcTMD (cyan) in complex with IL-7R TMD (grey), showing the positions of the mutations I265N, C278W and V279M, as well as the knob-into-hole interaction. (**B** and **C**) Quantification of cell surface expression level of human IL-7R and γc, respectively, by flow cytometry. Untransfected (Empty) BaF3 cells were used as negative controls. (**D**) Bar graphs showing mean fluorescence intensity for IL-7R surface expression. The data are means ± SEM from three independent experiments. Statistical significance: Student's *t* test; ns, not significant; ****$P \leq 0.0001$. (**E**) Bar graphs showing mean fluorescence intensity for γc surface expression. The data are means ± SEM from three independent experiments. Statistical significance: Student's *t* test; ns, not significant; ***$P \leq 0.001$. (**F and G**) Phosphorylation of STAT5 in BaF3 cells coexpressing WT hIL-7R with WT hγc or hγc mutants after 5h of cytokine deprivation and treatment with 30 or 50 ng/ml of hIL-7 (left and right lane, respectively). (**H**) BACTH analysis of the effect of hγc TMD mutations (G268R, M270R, I274T, C278W, V279M, I265N) on TMD heterodimerization.

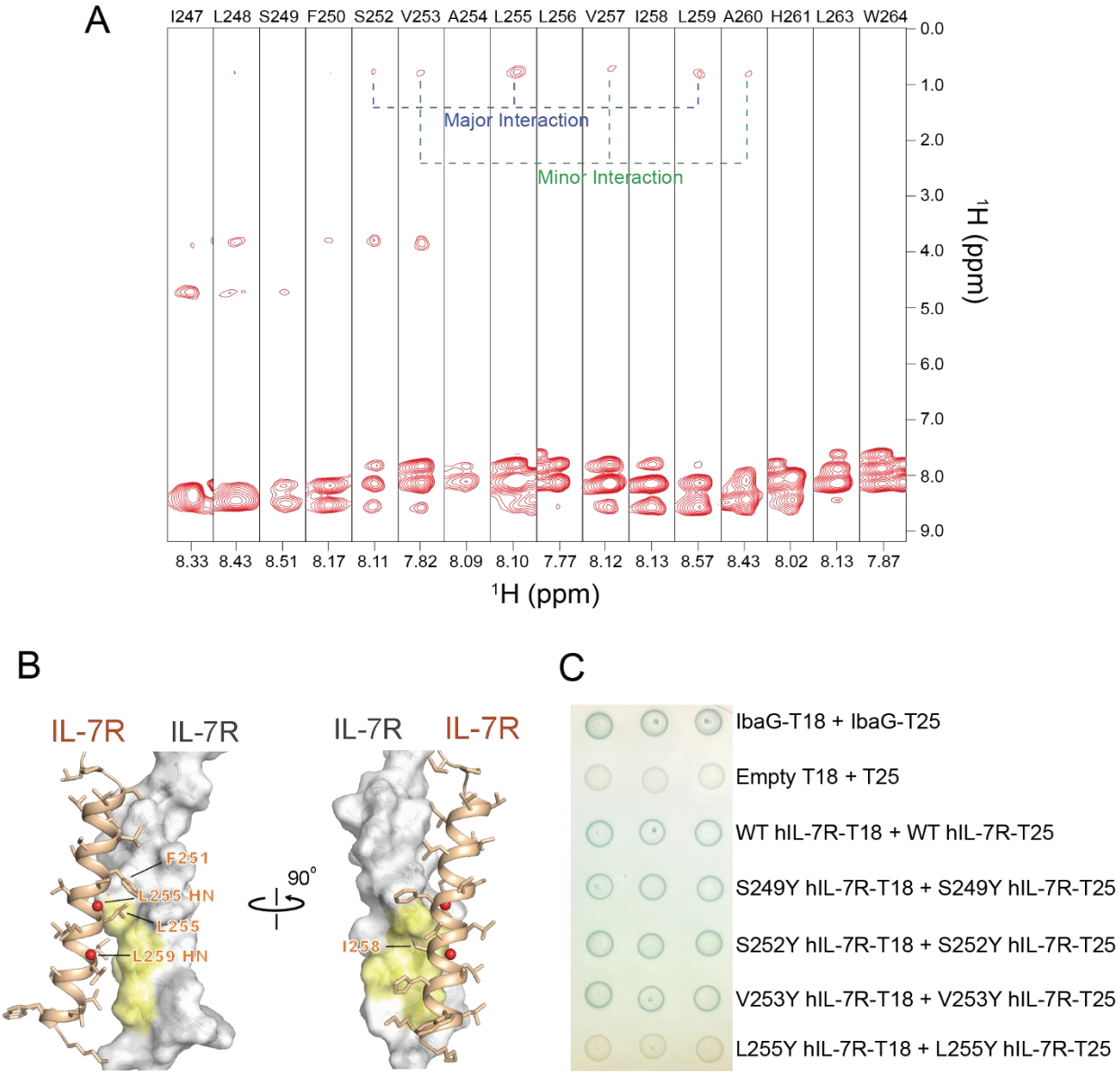

fig. S14. NMR analysis of self-association of human IL-7RTMD (hIL-7RTMD) in bicelles

(**A**) Strips from 3D ^{13}C-filtered/^{15}N-edited NOESY-TROSY spectra of (^{15}N, ^{13}C, ^{2}H)-labeled hIL-7RTMD randomly mixed with unlabeled hIL-7RTMD, recorded with τ_{NOE} = 200 ms at 303 K and ^{1}H frequency of 700 MHz. The bicelle was composed of deuterated DMPC and DH_6PC at a DMPC/DH_6PC ratio of 0.4. Intermolecular NOEs indicate two non-overlapping interactions. The major interaction yielding strong intermolecular NOEs involves the helix face with L255, I258, and L259. The minor interaction yielding weak NOEs involves the face with V253, V257, and A260. (**B**) Modeling of the major interaction based on NOEs in (A), showing that the self-

association of IL-7RTMD can be supported by good VDW surface complementarity involving residues F251, L255, and I258. (**C**) BACTH analysis of the effect of hIL-7RTMD mutations on hIL-7RTMD self-association.

Table S1. NMR structure calculation and refinement statistics

NMR distance and dihedral constraints [a]	γcTMD / IL-7RTMD	γcTMD / IL-9RTMD
Distance constraints from NOE	248	230
Short-range intramolecular ($\|i-j\| \leq 4$)	226	214
Long-range intramolecular ($\|i-j\| \geq 5$)	0	0
Intermolecular	22	16
Total dihedral angle restraints [b]	94	100
ϕ (TALOS)	47	50
ψ (TALOS)	47	50
Structure statistics [c]		
Violations (mean ± s.d.)		
Distance constraints (Å)	0.079 ± 0.004	0.054 ± 0.004
Dihedral angle constraints (º)	0.210 ± 0.042	0.335 ± 0.024
Deviations from idealized geometry		
Bond lengths (Å)	0.006 ± 0.000	0.006 ± 0.000
Bond angles (º)	0.284 ± 0.037	0.687 ± 0.012
Impropers (º)	0.434 ± 0.022	0.450 ± 0.020
Average pairwise r.m.s. deviation (Å) [d]		
Heavy	1.234	1.281
Backbone	0.645	0.711

[a] The numbers of restraints for the γcTMD–IL-7RTMD complex are summed over residues 257-285 of γcTMD and residues 246-266 of IL-7RTMD. The numbers of restraints for the γcTMD–IL-9RTMD complex are summed over residues 258-285 of γcTMD and residues 271-297 of IL-9RTMD.

[b] Backbone ϕ and ψ restraints and their respective uncertainties were obtained from the "GOOD" dihedrals generated by the TALOS+ program (*52*) based on the backbone chemical shift values.

[c] Statistics are calculated and averaged over an ensemble of the 15 lowest energy structures out of 100 calculated structures.

[d] The precision of the atomic coordinates is defined as the average r.m.s. difference between the 15 final structures and their mean coordinates. The calculation only includes the ordered regions of the protein: γcTMD residues 262-284 and IL-7RTMD residues 245-265 of the γcTMD–IL-7RTMD complex; γcTMD residues 262-284 and IL-9RTMD residues 271-293 of the γcTMD–IL-9RTMD complex.

Table S2. Cell lines, plasmids and reagents used in this study

Reagent or Resource	Source	Identifier
Antibodies		
Phospho-STAT5 (Tyr694) (C11C5) Rabbit mAb	Cell Signaling Technology	#9359
Phospho-Jak1(Y1034/1035) (D7N4Z) Rabbit mAb	Cell Signaling Technology	#74129
Phospho-Jak3 (Y980/981) (D44E3) Rabbit mAb	Cell Signaling Technology	#5031
STAT5 (D2O6Y) Rabbit mAb	Cell Signaling Technology	#94205
Beta-actin (13E5) Rabbit mAb	Cell signaling	#4970S
Anti-rabbit IgG-HRP linked Ab	Cell signaling	#7074S
Pacific blue-conjugated anti-hIL-7R (A019D5) mAb	BioLegend	#351306
APC-conjugated anti-hγc (TUGh4) mAb	BioLegend	#338608
anti-hIL-7(ZY335) mAb	AbboMax	#604-760
APC-conjugated anti-rat IgG (H+L) Ab	Invitrogen	#A10540
Bacterial Strains and mammalian cells		
E. coli BL21(DE3)	New England Biolabs	Cat# C2527
E. coli DH5-alpha	New England Biolabs	Cat# C2987
E. coli C43 (DE3)	Sigma-Aldrich	CMC0019
BTH101	Euromedex	EUB001
HEK293T	ATCC	CRL-3216; RRID: CVCL_0063
BaF3	AcceGen Biotech	ABC-TC060S
Chemicals, Peptides, and Recombinant Proteins		
Cyanogen Bromide	Sigma-Aldrich	Cat# C91492
Deuterium oxide	Cambridge Isotope Laboratories (CIL)	DLM-4-99.8-1000

^{13}C D-Glucose	CIL	CLM-13965
D1,2,3,4,5,6,7 D-Glucose	CIL	DLM-20621
^{15}N ammonium chloride	CIL	NLM-467-5
Kanamycin monosulfate	Sigma-Aldrich	Cat# BP861
Ampicillin, Sodium Salt	Sigma-Aldrich	Cat# 171254
isopropyl b-D-thiogalatopyranoside (IPTG)	Sigma-Aldrich	Cat# I5502
DMPC Lipid	Avanti Polar Lipids	Cat# 850345
DH6PC Detergent	Avanti Polar Lipids	Cat# 850305
Deuterated d54-DMPC lipid	Cortecnet	CD5012P025
Deuterated d22-DH6PC Detergent	Cortecnet	CD5010P025
Recombinant mouse IL-3	SIGMA-ALDRICH	#SRP3208-10UG
Recombinant human IL-7	Thermo Fisher Scientific	#PHC0075
TEV enzyme	James Chou lab	N/A
DAPI	Abcam	#ab228549
Polybrene	Sigma-Aldrich	#H9268
Retro-X™ Concentrator	Takara	#631455
RPMI 1640 medium	Thermo Fisher Scientific	# 11875119
DMEM	Gibco	#10566-016
Fetal bovine serum	Thermo Fisher Scientific	# 10082147
Penicillin-Streptomycin	Thermo Fisher Scientific	#15140122
DPBS	Gibco	#14190-144
Trypsin-EDTA	Gibco	# 25200056
Lipofectamine™ 3000	Thermo Fisher Scientific	# L3000008
Opti-MEM	Gibco	#31985-062
X-Gal	AdipoGen	#AG-CC1-0003
Vectors and plasmids		

pKNT25	Euromedex	EUP-25N
pUT18	Euromedex	EUP-18N
IbaG-pKNT25	A. Zoued (Harvard Medical School)	N/A
IbaG- pUT18	A. Zoued (Harvard Medical School)	N/A
OmpA-mIL-7RTD-pKNT25	This paper	N/A
OmpA-mIL-7RTMD-pUT18	This paper	N/A
OmpA-hIL-7RTMD-pKNT25	This paper	N/A
OmpA-hIL-7RTMD-pUT18	This paper	N/A
OmpA-mγcTMD-pKNT25	This paper	N/A
OmpA-mγcTMD-pUT18	This paper	N/A
OmpA-hγcTMD-pKNT25	This paper	N/A
OmpA-hγcTMD-UT18	This paper	N/A
OmpA-mIL-4RTMD-pKNT25	This paper	N/A
OmpA-mIL-4RTMD-pUT18	This paper	N/A
OmpA-hIL-4RTMD-pKNT25	This paper	N/A
OmpA-hIL-4RTMD-pUT18	This paper	N/A
OmpA-mIL-9RTMD-pKNT25	This paper	N/A
OmpA-mIL-9RTMD-pUT18	This paper	N/A
OmpA-hIL-9RTMD-pKNT25	This paper	N/A
OmpA-hIL-9RTMD-pUT18	This paper	N/A
OmpA-mIL-5RTMD-pKNT25	This paper	N/A
OmpA-mIL-5RTMD-pUT18	This paper	N/A
OmpA-hIL-5RTMD-pKNT25	This paper	N/A
OmpA-hIL-5RTMD-pUT18	This paper	N/A
OmpA-hIL-2RαTMD-pKNT25	This paper	N/A
OmpA-hIL-2RαTMD-pUT18	This paper	N/A
OmpA-hIL-2RβTMD-pKNT25	This paper	N/A
OmpA-hIL-2RβTMD-pUT18	This paper	N/A

OmpA-hIL-15RTMD-pKNT25	This paper	N/A
OmpA-hIL-15RTMD-pUT18	This paper	N/A
OmpA-hIL-21RTMD-pKNT25	This paper	N/A
OmpA-hIL-21RTMD-pUT18	This paper	N/A
OmpA-hIL-βcTMD-pKNT25	This paper	N/A
OmpA-hIL-βcTMD-pUT18	This paper	N/A
OmpA-S249Y hIL-7RTMD-pKNT25	This paper	N/A
OmpA-S249Y hIL-7RTMD-pUT18	This paper	N/A
OmpA-S252Y hIL-7RTMD-pKNT25	This paper	N/A
OmpA-S252Y hIL-7RTMD-pUT18	This paper	N/A
OmpA-V253Y hIL-7RTMD-pKNT25	This paper	N/A
OmpA-V253Y hIL-7RTMD-pUT18	This paper	N/A
OmpA-L255Y hIL-7RTMD-pKNT25	This paper	N/A
OmpA-L255Y hIL-7RTMD-pUT18	This paper	N/A
OmpA-P267Y mγcTMD-pKNT25	This paper	N/A
OmpA-P267Y mγcTMD-pUT18	This paper	N/A
OmpA-T270Y mγcTMD-pKNT25	This paper	N/A
OmpA-T270Y mγcTMD-pUT18	This paper	N/A
OmpA-G272Y mγcTMD-pKNT25	This paper	N/A
OmpA-G272Y mγcTMD-pUT18	This paper	N/A
OmpA-L273Y mγcTMD-pKNT25	This paper	N/A
OmpA-L273Y mγcTMD-pUT18	This paper	N/A
OmpA-I274Y mγcTMD-pKNT25	This paper	N/A
OmpA-I274Y mγcTMD-pUT18	This paper	N/A
OmpA-L277Y mγcTMD-pKNT25	This paper	N/A
OmpA-L277Y mγcTMD-pUT18	This paper	N/A
OmpA-S266Y hγcTMD-pKNT25	This paper	N/A
OmpA-S266Y hγcTMD-pUT18	This paper	N/A
OmpA-S269Y hγcTMD-pKNT25	This paper	N/A
OmpA-S269Y hγcTMD-pUT18	This paper	N/A

OmpA-G271Y hγcTMD-pKNT25	This paper	N/A
OmpA-G271Y hγcTMD-pUT18	This paper	N/A
OmpA-L272Y hγcTMD-pKNT25	This paper	N/A
OmpA-L272Y hγcTMD-pUT18	This paper	N/A
OmpA-I273Y hγcTMD-pKNT25	This paper	N/A
OmpA-I273Y hγcTMD-UT18	This paper	N/A
OmpA-L276Y hγcTMD-pKNT25	This paper	N/A
OmpA-L276Y hγcTMD-UT18	This paper	N/A
OmpA-S249Y mIL-7RTMD-pKNT25	This paper	N/A
OmpA- S249Y mIL-7RTMD-pUT18	This paper	N/A
OmpA-S252Y mIL-7RTMD-pKNT25	This paper	N/A
OmpA- S252Y mIL-7RTMD-pUT18	This paper	N/A
OmpA-V253G mIL-7RTMD-pKNT25	This paper	N/A
OmpA- V253G mIL-7RTMD-pUT18	This paper	N/A
OmpA-V253Y mIL-7RTMD-pKNT25	This paper	N/A
OmpA- V253Y mIL-7RTMD-pUT18	This paper	N/A
OmpA-L255Y mIL-7RTMD-pKNT25	This paper	N/A
OmpA- L255Y mIL-7RTMD-pUT18	This paper	N/A
OmpA-V257Y mIL-7RTMD-pKNT25	This paper	N/A
OmpA- V257Y mIL-7RTMD-pUT18	This paper	N/A
MSCV-hIL-7R-EGFP	This paper	N/A
MSCV-hIL-7R TEV-EGFP	This paper	N/A
MSCV-hIL-7R V253Y-EGFP	This paper	N/A
MSCV-hIL-7R L255Y-EGFP	This paper	N/A
MSCV-hIL-7R-ΔECD-EGFP	This paper	N/A
MSCV- hγc-mCherry	This paper	N/A
MSCV- hγc TEV-mCherry	This paper	N/A
MSCV- hγc G271Y-mCherry	This paper	N/A
MSCV- hγc I273Y-mCherry	This paper	N/A
MSCV- hγc G268R-mCherry	This paper	N/A

MSCV- hγc M270R-mCherry	This paper	N/A
MSCV- hγc I274T-mCherry	This paper	N/A
MSCV- hγc C278W-mCherry	This paper	N/A
MSCV- hγc V279M-mCherry	This paper	N/A
MSCV- hγc I265N-mCherry	This paper	N/A
MSCV- hγc-ΔECD -mCherry	This paper	N/A
MSCV-hIL-9R-EGFP	This paper	N/A
MSCV-hIL-9R TEV-EGFP	This paper	N/A
MSCV-hIL-9R L282Y-EGFP	This paper	N/A
MSCV-hIL-9R T284Y-EGFP	This paper	N/A
pMM-LR6 -His-TrpLE-mγcTMD	This paper	N/A
pMM-LR6 -His-TrpLE-mIL-7RTMD	This paper	N/A
pMM-LR6 -His-TrpLE-mIL-9RTMD	This paper	N/A
pMM-LR6 -His-TrpLE-hIL-7RTMD	This paper	N/A

References and Notes

1. W. J. Leonard, Cytokines and immunodeficiency diseases. *Nat. Rev. Immunol.* **1**, 200–208 (2001). doi:10.1038/35105066 Medline

2. Y. Rochman, R. Spolski, W. J. Leonard, New insights into the regulation of T cells by γ_c family cytokines. *Nat. Rev. Immunol.* **9**, 480–490 (2009). doi:10.1038/nri2580 Medline

3. R. Spolski, W. J. Leonard, Interleukin-21: Basic biology and implications for cancer and autoimmunity. *Annu. Rev. Immunol.* **26**, 57–79 (2008). doi:10.1146/annurev.immunol.26.021607.090316 Medline

4. J.-X. Lin, W. J. Leonard, The Common Cytokine Receptor γ Chain Family of Cytokines. *Cold Spring Harb. Perspect. Biol.* **10**, a028449 (2018). doi:10.1101/cshperspect.a028449 Medline

5. W. J. Leonard, J. X. Lin, J. J. O'Shea, The γ_c Family of Cytokines: Basic Biology to Therapeutic Ramifications. *Immunity* **50**, 832–850 (2019). doi:10.1016/j.immuni.2019.03.028 Medline

6. X. Wang, M. Rickert, K. C. Garcia, Structure of the quaternary complex of interleukin-2 with its α, β, and γ_c receptors. *Science* **310**, 1159–1163 (2005). doi:10.1126/science.1117893 Medline

7. X. Wang, P. Lupardus, S. L. Laporte, K. C. Garcia, Structural biology of shared cytokine receptors. *Annu. Rev. Immunol.* **27**, 29–60 (2009). doi:10.1146/annurev.immunol.24.021605.090616 Medline

8. S. L. LaPorte, Z. S. Juo, J. Vaclavikova, L. A. Colf, X. Qi, N. M. Heller, A. D. Keegan, K. C. Garcia, Molecular and structural basis of cytokine receptor pleiotropy in the interleukin-4/13 system. *Cell* **132**, 259–272 (2008). doi:10.1016/j.cell.2007.12.030 Medline

9. K. F. Kubatzky, W. Ruan, R. Gurezka, J. Cohen, R. Ketteler, S. S. Watowich, D. Neumann, D. Langosch, U. Klingmüller, Self assembly of the transmembrane domain promotes signal transduction through the erythropoietin receptor. *Curr. Biol.* **11**, 110–115 (2001). doi:10.1016/S0960-9822(01)00018-5 Medline

10. E. E. Matthews, D. Thévenin, J. M. Rogers, L. Gotow, P. D. Lira, L. A. Reiter, W. H. Brissette, D. M. Engelman, Thrombopoietin receptor activation: Transmembrane helix dimerization, rotation, and allosteric modulation. *FASEB J.* **25**, 2234–2244 (2011). doi:10.1096/fj.10-178673 Medline

11. N. Yang, X. Wang, J. Jiang, S. J. Frank, Role of the growth hormone (GH) receptor transmembrane domain in receptor predimerization and GH-induced activation. *Mol. Endocrinol.* **21**, 1642–1655 (2007). doi:10.1210/me.2006-0458 Medline

12. E. V. Bocharov, D. M. Lesovoy, O. V. Bocharova, A. S. Urban, K. V. Pavlov, P. E. Volynsky, R. G. Efremov, A. S. Arseniev, Structural basis of the signal transduction via transmembrane domain of the human growth hormone receptor. *Biochim. Biophys. Acta Gen. Subj.* **1862**, 1410–1420 (2018). doi:10.1016/j.bbagen.2018.03.022 Medline

13. Q. Fu, T.-M. Fu, A. C. Cruz, P. Sengupta, S. K. Thomas, S. Wang, R. M. Siegel, H. Wu, J. J. Chou, Structural Basis and Functional Role of Intramembrane Trimerization of the

Fas/CD95 Death Receptor. *Mol. Cell* **61**, 602–613 (2016). doi:10.1016/j.molcel.2016.01.009 Medline

14. L. Pan, T.-M. Fu, W. Zhao, L. Zhao, W. Chen, C. Qiu, W. Liu, Z. Liu, A. Piai, Q. Fu, S. Chen, H. Wu, J. J. Chou, Higher-Order Clustering of the Transmembrane Anchor of DR5 Drives Signaling. *Cell* **176**, 1477–1489.e14 (2019). doi:10.1016/j.cell.2019.02.001 Medline

15. A. Arkhipov, Y. Shan, R. Das, N. F. Endres, M. P. Eastwood, D. E. Wemmer, J. Kuriyan, D. E. Shaw, Architecture and membrane interactions of the EGF receptor. *Cell* **152**, 557–569 (2013). doi:10.1016/j.cell.2012.12.030 Medline

16. N. F. Endres, R. Das, A. W. Smith, A. Arkhipov, E. Kovacs, Y. Huang, J. G. Pelton, Y. Shan, D. E. Shaw, D. E. Wemmer, J. T. Groves, J. Kuriyan, Conformational coupling across the plasma membrane in activation of the EGF receptor. *Cell* **152**, 543–556 (2013). doi:10.1016/j.cell.2012.12.032 Medline

17. G. Skiniotis, P. J. Lupardus, M. Martick, T. Walz, K. C. Garcia, Structural organization of a full-length gp130/LIF-R cytokine receptor transmembrane complex. *Mol. Cell* **31**, 737–748 (2008). doi:10.1016/j.molcel.2008.08.011 Medline

18. C. Shochat, N. Tal, V. Gryshkova, Y. Birger, O. R. Bandapalli, G. Cazzaniga, N. Gershman, A. E. Kulozik, A. Biondi, M. R. Mansour, J.-C. Twizere, M. U. Muckenthaler, N. Ben-Tal, S. N. Constantinescu, D. Bercovich, S. Izraeli, Novel activating mutations lacking cysteine in type I cytokine receptors in acute lymphoblastic leukemia. *Blood* **124**, 106–110 (2014). doi:10.1182/blood-2013-10-529685 Medline

19. S. T. Walsh, Structural insights into the common γ-chain family of cytokines and receptors from the interleukin-7 pathway. *Immunol. Rev.* **250**, 303–316 (2012). doi:10.1111/j.1600-065X.2012.01160.x Medline

20. G. Du, L. Zhao, Y. Zheng, A. Belfetmi, T. Cai, B. Xu, K. Heyninck, K. Van Den Heede, M.-A. Buyse, P. Fontana, M. Bowman, L.-L. Lin, H. Wu, J. J. Chou, Autoinhibitory structure of preligand association state implicates a new strategy to attain effective DR5 receptor activation. *Cell Res.* **33**, 131–146 (2023). doi:10.1038/s41422-022-00755-2 Medline

21. C. A. McElroy, P. J. Holland, P. Zhao, J.-M. Lim, L. Wells, E. Eisenstein, S. T. R. Walsh, Structural reorganization of the interleukin-7 signaling complex. *Proc. Natl. Acad. Sci. U.S.A.* **109**, 2503–2508 (2012). doi:10.1073/pnas.1116582109 Medline

22. P. Gonnord, B. R. Angermann, K. Sadtler, E. Gombos, P. Chappert, M. Meier-Schellersheim, R. Varma, A hierarchy of affinities between cytokine receptors and the common gamma chain leads to pathway cross-talk. *Sci. Signal.* **11**, eaal1253 (2018). doi:10.1126/scisignal.aal1253 Medline

23. A. T. Waickman, H. R. Keller, T.-H. Kim, M. A. Luckey, X. Tai, C. Hong, C. Molina-París, S. T. R. Walsh, J.-H. Park, The Cytokine Receptor IL-7Rα Impairs IL-2 Receptor Signaling and Constrains the *In Vitro* Differentiation of Foxp3^{+} Treg Cells. *iScience* **23**, 101421 (2020). doi:10.1016/j.isci.2020.101421 Medline

24. K. R. MacKenzie, J. H. Prestegard, D. M. Engelman, A transmembrane helix dimer: Structure and implications. *Science* **276**, 131–133 (1997). doi:10.1126/science.276.5309.131 Medline

25. E. V. Bocharov, K. S. Mineev, P. E. Volynsky, Y. S. Ermolyuk, E. N. Tkach, A. G. Sobol, V. V. Chupin, M. P. Kirpichnikov, R. G. Efremov, A. S. Arseniev, Spatial structure of the dimeric transmembrane domain of the growth factor receptor ErbB2 presumably corresponding to the receptor active state. *J. Biol. Chem.* **283**, 6950–6956 (2008). doi:10.1074/jbc.M709202200 Medline

26. R. Trenker, M. E. Call, M. J. Call, Crystal Structure of the Glycophorin A Transmembrane Dimer in Lipidic Cubic Phase. *J. Am. Chem. Soc.* **137**, 15676–15679 (2015). doi:10.1021/jacs.5b11354 Medline

27. M. E. Call, K. W. Wucherpfennig, Common themes in the assembly and architecture of activating immune receptors. *Nat. Rev. Immunol.* **7**, 841–850 (2007). doi:10.1038/nri2186 Medline

28. M. E. Call, K. W. Wucherpfennig, J. J. Chou, The structural basis for intramembrane assembly of an activating immunoreceptor complex. *Nat. Immunol.* **11**, 1023–1029 (2010). doi:10.1038/ni.1943 Medline

29. L. K. Fong, M. J. Chalkley, S. K. Tan, M. Grabe, W. F. DeGrado, Elucidation of the molecular interactions that enable stable assembly and structural diversity in multicomponent immune receptors. *Proc. Natl. Acad. Sci. U.S.A.* **118**, e2026318118 (2021). doi:10.1073/pnas.2026318118 Medline

30. A. Battesti, E. Bouveret, The bacterial two-hybrid system based on adenylate cyclase reconstitution in *Escherichia coli*. *Methods* **58**, 325–334 (2012). doi:10.1016/j.ymeth.2012.07.018 Medline

31. S. Damjanovich, L. Bene, J. Matkó, A. Alileche, C. K. Goldman, S. Sharrow, T. A. Waldmann, Preassembly of interleukin 2 (IL-2) receptor subunits on resting Kit 225 K6 T cells and their modulation by IL-2, IL-7, and IL-15: A fluorescence resonance energy transfer study. *Proc. Natl. Acad. Sci. U.S.A.* **94**, 13134–13139 (1997). doi:10.1073/pnas.94.24.13134 Medline

32. J. M. Puck, A. E. Pepper, P. S. Henthorn, F. Candotti, J. Isakov, T. Whitwam, M. E. Conley, R. E. Fischer, H. M. Rosenblatt, T. N. Small, R. H. Buckley, Mutation analysis of IL2RG in human X-linked severe combined immunodeficiency. *Blood* **89**, 1968–1977 (1997). doi:10.1182/blood.V89.6.1968 Medline

33. J. E. Niemela, J. M. Puck, R. E. Fischer, T. A. Fleisher, A. P. Hsu, Efficient detection of thirty-seven new *IL2RG* mutations in human X-linked severe combined immunodeficiency. *Clin. Immunol.* **95**, 33–38 (2000). doi:10.1006/clim.2000.4846 Medline

34. C. M. Yao, X.-H. Han, Y.-D. Zhang, H. Zhang, Y.-Y. Jin, R.-M. Cao, X. Wang, Q.-H. Liu, W. Zhao, T.-X. Chen, Clinical characteristics and genetic profiles of 44 patients with severe combined immunodeficiency (SCID): Report from Shanghai, China (2004–2011). *J. Clin. Immunol.* **33**, 526–539 (2013). doi:10.1007/s10875-012-9854-1 Medline

35. I. V. Korendovych, W. F. DeGrado, *De novo* protein design, a retrospective. *Q. Rev. Biophys.* **53**, e3 (2020). doi:10.1017/S0033583519000131 Medline

36. P. Lu, D. Min, F. DiMaio, K. Y. Wei, M. D. Vahey, S. E. Boyken, Z. Chen, J. A. Fallas, G. Ueda, W. Sheffler, V. K. Mulligan, W. Xu, J. U. Bowie, D. Baker, Accurate

computational design of multipass transmembrane proteins. *Science* **359**, 1042–1046 (2018). doi:10.1126/science.aaq1739 Medline

37. P. Barth, A. Senes, Toward high-resolution computational design of the structure and function of helical membrane proteins. *Nat. Struct. Mol. Biol.* **23**, 475–480 (2016). doi:10.1038/nsmb.3231 Medline

38. H. Yin, J. S. Slusky, B. W. Berger, R. S. Walters, G. Vilaire, R. I. Litvinov, J. D. Lear, G. A. Caputo, J. S. Bennett, W. F. DeGrado, Computational design of peptides that target transmembrane helices. *Science* **315**, 1817–1822 (2007). doi:10.1126/science.1136782 Medline

39. A. Elazar, N. J. Chandler, A. S. Davey, J. Y. Weinstein, J. V. Nguyen, R. Trenker, R. S. Cross, M. R. Jenkins, M. J. Call, M. E. Call, S. J. Fleishman, De novo-designed transmembrane domains tune engineered receptor functions. *eLife* **11**, e75660 (2022). doi:10.7554/eLife.75660 Medline

40. A. Fleurie, A. Zoued, L. Alvarez, K. M. Hines, F. Cava, L. Xu, B. M. Davis, M. K. Waldor, A *Vibrio cholerae* BolA-Like Protein Is Required for Proper Cell Shape and Cell Envelope Integrity. *mBio* **10**, e00790-19 (2019). doi:10.1128/mBio.00790-19 Medline

41. C. A. Schneider, W. S. Rasband, K. W. Eliceiri, NIH Image to ImageJ: 25 years of image analysis. *Nat. Methods* **9**, 671–675 (2012). doi:10.1038/nmeth.2089 Medline

42. J. Qu, Z. Yang, Protocol to produce high-titer retrovirus for transduction of mouse bone marrow cells. *STAR Protoc.* **2**, 100459 (2021). doi:10.1016/j.xpro.2021.100459 Medline

43. T. Murakami, J. Kim, Y. Li, G. E. Green, A. Shikanov, A. Ono, Secondary lymphoid organ fibroblastic reticular cells mediate trans-infection of HIV-1 via CD44-hyaluronan interactions. *Nat. Commun.* **9**, 2436 (2018). doi:10.1038/s41467-018-04846-w Medline

44. P. P. Zenatti, D. Ribeiro, W. Li, L. Zuurbier, M. C. Silva, M. Paganin, J. Tritapoe, J. A. Hixon, A. B. Silveira, B. A. Cardoso, L. M. Sarmento, N. Correia, M. L. Toribio, J. Kobarg, M. Horstmann, R. Pieters, S. R. Brandalise, A. A. Ferrando, J. P. Meijerink, S. K. Durum, J. A. Yunes, J. T. Barata, Oncogenic IL7R gain-of-function mutations in childhood T-cell acute lymphoblastic leukemia. *Nat. Genet.* **43**, 932–939 (2011). doi:10.1038/ng.924 Medline

45. Q. Fu, A. Piai, W. Chen, K. Xia, J. J. Chou, Structure determination protocol for transmembrane domain oligomers. *Nat. Protoc.* **14**, 2483–2520 (2019). doi:10.1038/s41596-019-0188-9 Medline

46. F. Delaglio, S. Grzesiek, G. W. Vuister, G. Zhu, J. Pfeifer, A. Bax, NMRPipe: A multidimensional spectral processing system based on UNIX pipes. *J. Biomol. NMR* **6**, 277–293 (1995). doi:10.1007/BF00197809 Medline

47. C. Bartels, T.-h. Xia, M. Billeter, P. Güntert, K. Wüthrich, The program XEASY for computer-supported NMR spectral analysis of biological macromolecules. *J. Biomol. NMR* **6**, 1–10 (1995). doi:10.1007/BF00417486 Medline

48. W. F. Vranken, W. Boucher, T. J. Stevens, R. H. Fogh, A. Pajon, M. Llinas, E. L. Ulrich, J. L. Markley, J. Ionides, E. D. Laue, The CCPN data model for NMR spectroscopy:

Development of a software pipeline. *Proteins* **59**, 687–696 (2005). doi:10.1002/prot.20449 Medline

49. L. E. Kay, M. Ikura, R. Tschudin, A. Bax, Three-dimensional triple-resonance NMR Spectroscopy of isotopically enriched proteins. *J. Magn. Reson.* **213**, 423–441 (2011). doi:10.1016/j.jmr.2011.09.004 Medline

50. M. Salzmann, G. Wider, K. Pervushin, H. Senn, K. Wüthrich, TROSY-type Triple-Resonance Experiments for Sequential NMR Assignments of Large Proteins. *J. Am. Chem. Soc.* **121**, 844–848 (1999). doi:10.1021/ja9834226

51. C. D. Schwieters, J. J. Kuszewski, N. Tjandra, G. M. Clore, The Xplor-NIH NMR molecular structure determination package. *J. Magn. Reson.* **160**, 65–73 (2003). doi:10.1016/S1090-7807(02)00014-9 Medline

52. Y. Shen, F. Delaglio, G. Cornilescu, A. Bax, TALOS+: A hybrid method for predicting protein backbone torsion angles from NMR chemical shifts. *J. Biomol. NMR* **44**, 213–223 (2009). doi:10.1007/s10858-009-9333-z Medline

53. J. S. Papadopoulos, R. Agarwala, COBALT: Constraint-based alignment tool for multiple protein sequences. *Bioinformatics* **23**, 1073–1079 (2007). doi:10.1093/bioinformatics/btm076 Medline